

Validation of classical density-dependent solute transport theory for stable, high-concentration-gradient brine displacements in coarse and medium sands

S.J. Watson ^{a,1}, D.A. Barry ^{a,1}, R.J. Schotting ^{b,*}, S.M. Hassanizadeh ^b

^a School of Civil and Environmental Engineering, Contaminated Land Assessment and Remediation Research Centre, The University of Edinburgh, Edinburgh EH9 3JN, UK

^b Department of Water Management, Faculty of Civil Engineering and Geosciences, Delft University of Technology, P.O. Box 5048, 2600 GA Delft, The Netherlands

Received 21 March 2001; received in revised form 1 February 2002; accepted 28 February 2002

Abstract

A series of careful laboratory soil column experiments was carried out for the purpose of providing data for testing recently presented theories of miscible density-dependent flow and transport. In particular, modifications to the standard theory involve extensions to both Darcy's (for flow) and Fick's laws (for diffusive/dispersive solute flux). Both coarse- and medium-grained sands were used in the experiments. All experiments concerned upward (i.e., stable) displacement of fresh water within the soil by a brine solution, under either constant head or constant volume flux conditions. The experimental data were analysed using accurate numerical solutions of the standard governing flow and transport model, as well as models with modified Darcy's and Fick's laws. Model parameters were determined by a step-wise fitting procedure based on the least-squares criterion. The results show clearly that, for large density contrasts, an extended Darcy's law was not necessary. On the other hand, an extension to Fick's Law was needed to model the experimental data accurately.

© 2002 Published by Elsevier Science Ltd.

1. Introduction

Although the effect of density on solute transport has been researched for many years, significantly less experimental research has been conducted to investigate high-concentration (e.g., brine) solute transport through porous media. Even in the case where there are no solute–sediment interactions, the transport parameters characterising high concentration transport exhibit more complex behaviour than for low-concentration transport, due to concentration-dependent changes in viscosity and density.

Displacements may be stable or unstable, depending on viscosity and density differences between the displaced and displacing liquids [13]. For brine, increased salt concentration leads to increased viscosity and den-

sity. For upward displacements of salt-free solution by brine (the case considered here), the displacing front is always stable.

For stable displacements, several authors have reported experiments looking at the mixing zone in the interface of the displaced solution and displacing solution [6,24,25]. These experiments show consistently that, for the stable displacements referred to above, an increase in the density or viscosity contrast leads to a reduced mixing zone. Thus, in macroscopic terms, the hydrodynamic dispersion coefficient will vary with these contrasts.

Hassanizadeh et al. [9] presented the results from a series of laboratory experiments investigating stable high concentration displacements through a uniform porous media. Glass beads of diameter 0.4–0.52 mm were packed between two Plexiglass plates, 1 cm apart, under wet conditions. One-dimensional, vertical displacement tests were conducted with flow in an upwards direction. Constant influent and effluent fluid levels were maintained during the displacements, resulting in a varying flow rate during the high concentration

* Corresponding author. Tel.: +31-15-278-4844/5074; fax: +31-15-278-5915.

E-mail address: r.j.schotting@ct.tudelft.nl (R.J. Schotting).

¹ Tel.: +44-131-650-7204; fax: +44-131-650-7276.

displacements. Both low and high concentration stable displacements were conducted.

Hassanizadeh et al. [8] investigated the applicability of Darcy's and Fick's laws to the high concentration displacement results presented in [9]. The classical formulations of these laws were used for calibration purposes to evaluate porosity and dispersivity values for the porous medium from the breakthrough curves of a low concentration displacement. The hydrodynamic dispersion coefficient was assumed to be linearly dependent on the fluid flux, and the longitudinal dispersivity of the porous medium was used for the analysis. The intrinsic permeability of the medium was determined from independent experiments. These values were then used to predict the breakthrough curves from a second low concentration displacement and two high concentration displacements. Satisfactory agreement was obtained between the experimental and calculated breakthrough curves for the low concentration displacement, however the agreement was poor for the high concentration displacements. The results indicated that the classical formulation of Fick's law predicted greater dispersion of the solute front than actually occurred in the high concentration displacements. Hassanizadeh [9] then investigated the applicability of a number of modified versions of Fick's law and presented a nonlinear relationship for the dispersive solute flux that most accurately predicted the experimental results. The nonlinear dispersion equation is given by:

$$(1 + \beta|J|)J = -\rho n D_h \frac{\partial \omega}{\partial z}, \quad (1)$$

where β is a new material coefficient, in addition to the hydrodynamic dispersion coefficient, D_h . In (1), J denotes dispersive mass flux, n is porosity, ρ is fluid density, and ω is salt mass fraction. A physical interpretation of the underlying phenomenon is given in [23]. For $\beta = 0$, (1) reduces to Fick's law. Subsequently, [11] presented a nonlinear dispersion theory which was shown to predict both low and high concentration displacements for a unique set of parameter values. They found that good agreement of the experimental and calculated breakthrough curves was obtained.

A series of low and high concentration, stable displacement experiments were conducted by [19] to determine the influence of salt concentration on hydrodynamic dispersion in porous media. Solute breakthrough curves were measured using small conductivity

probes inserted into the soil within the column. The porous medium tested was a quartz sand which had a median grain size of 0.50 mm.

Schotting et al. [23] gave an extensive analysis of the data reported by [19], with a focus on the applicability of (1). One important result obtained by them was the variation of β with the Darcy flux, q . They showed that β showed a power-law behaviour as a function q , with values of β of order 10^5 for low flow rates, reducing to less than 10^3 for high flow rates. In their analysis, they assumed that Darcy's law was valid. On the other hand, several authors have proposed variations to both Darcy's law and Fick's law for stable high-concentration brine displacements. For example, [10,17] suggested that Darcy's law be extended to include a cross-coupling term to reflect the effect of flow induced by chemical osmosis:

$$q = -\frac{k}{\mu} \left(\frac{\partial p}{\partial z} + \rho g \right) - D^f \frac{\partial \omega}{\partial z}. \quad (2)$$

Here, q is specific discharge, k is intrinsic permeability, μ is viscosity, g is acceleration due to gravity, and ρ is fluid pressure. For $D^f = 0$, (2) reduces to Darcy's law. The cross-coupling coefficient, D^f , can be further decomposed, as discussed by [17]. It is worthwhile noting that its magnitude depends on the osmotic efficiency of the porous medium.

The objective of this paper is twofold:

1. To present extensive data on high-concentration brine displacements.
2. To test the validity of both Darcy's law and Fick's law.

Numerous experiments were performed, as presented in Table 1. Two types of sand were tested. For one type, i.e. coarse sand, two different inflow conditions were applied: constant head and constant flow rate. The constant head experiments provided data for verification purposes, while the constant flow rate data were used for parameter determination. The experiments were conducted in a laboratory column apparatus to investigate the effect of high solute concentration gradients on fluid flow and solute transport processes within saturated soils. The emphasis will be on the presentation of the experimental data. For two reasons, some modeling results are included. First of all, an important open question, related to the validity of classical Darcy law

Table 1
Outline of the three experimental test series

Test series	Sand type	Imposed flow condition	Number of displacements	Test names
I	Coarse	Constant head	12	CS1-5u-CS4-200u
II	Coarse	Constant flow	14	CS5-5u-CS10-200u
III	Medium	Constant flow	15	MS1-5u-MS7-200u

under high concentration (gradient) conditions, had to be addressed. Computer simulations were necessary to provide an answer to this question. Secondly, modeling was conducted in order to validate a nonlinear dispersion theory suggested by [8].

2. Theory

The governing one-dimensional equations comprising classical isothermal transport theory for density-dependent solute transport are given below (e.g., [26]).

Conservation-of-mass equations:

$$\frac{\partial(n\rho)}{\partial t} + \frac{\partial(\rho q)}{\partial z} = 0, \quad (3)$$

$$\frac{\partial(n\rho\omega)}{\partial t} + \frac{\partial(\rho\omega q)}{\partial z} + \frac{\partial J}{\partial z} = 0. \quad (4)$$

Conservation-of-flux equations:

Darcy's law, i.e., (2), with $D^f = 0$, Fick's law, i.e., (1), with $\beta = 0$.

Equations of state:

$$\rho = \rho_0 \exp(\gamma\omega), \quad (5)$$

$$\mu = \mu_0 (1.00 + 1.85\omega - 4.10\omega^2 + 44.5\omega^3). \quad (6)$$

In (5), the effect of pressure changes on density have been ignored as insignificant for the experiments analysed here (e.g., [10]). Also, [10] give $\gamma = 0.6923$. The reference states, $\rho_0 = 998.23 \text{ kg m}^{-3}$ and $\mu_0 = 10^{-3} \text{ N s m}^{-2}$, are for salt-free water as measured at 20 °C and 1 atm, conditions that are appropriate for our experiments.

2.1. Initial and boundary conditions

There are two transport equations to be solved, (3) for the liquid and (4) for the solute.

Initial conditions:

$$p = \rho_0 g z, \quad t = 0, \quad 0 < z < L_c, \quad (7)$$

$$\omega = 0, \quad t = 0, \quad 0 < z < L_c. \quad (8)$$

Eqs. (7) and (8) state that the column liquid was under hydrostatic conditions and solute-free at the beginning of each experiment.

Boundary conditions:

$$p = p_{\text{meas}}, \quad z = 0, \quad (9)$$

$$\omega = \omega_{\text{meas}}, \quad z = 0, L_c, \quad (10)$$

$$q = q_{\text{meas}}, \quad z = L_c, \quad (11)$$

$$\frac{\partial\omega}{\partial z} = 0, \quad z = L_c. \quad (12)$$

The influent pressure condition was measured, as given by (9), as was the concentration, (10). Note that the measurements at L1 (Fig. 1) were taken as $z = 0$ for all experiments analysed. Measurements of concentration at L6 (defines $z = L_c$ in all cases) and of effluent flux

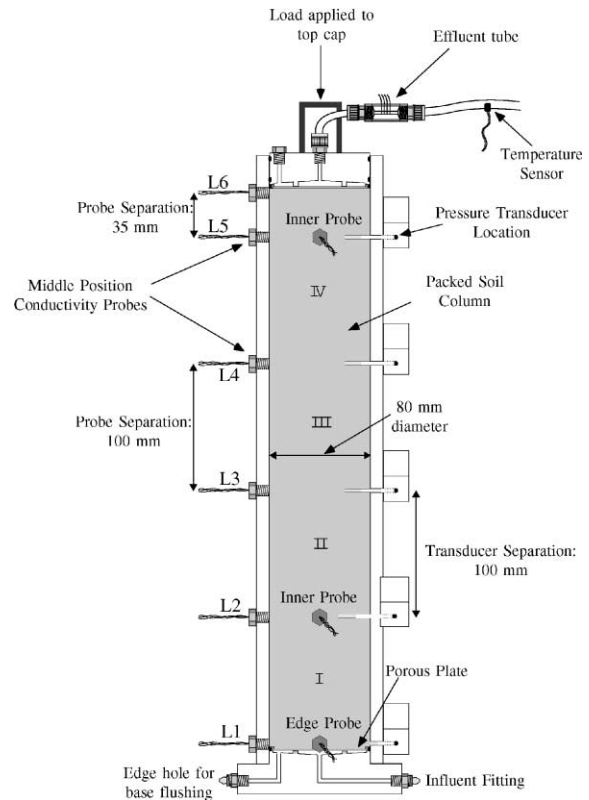


Fig. 1. Schematic diagram of the laboratory column apparatus.

were used as the exit boundary conditions, (10) and (11), except for the constant head tests, for which (12) was used as the solute effluent boundary condition.

3. Laboratory column apparatus and experimental procedure

The column apparatus was specifically designed for the displacement experiments to promote a uniform, one-dimensional flow regime within the column, and to minimise apparatus-induced dispersion. Saturated coarse and medium sands were tested. Influent solutions, ranging from 5 to 200 g l^{-1} of sodium chloride (NaCl), displaced salt-free pore water within the soil. A summary of the experimental conditions, and the designations of the various experiments reported here, is given in Table 1. The particular choice of the test names in Table 1 can be explained as follows: CS1-5u refers to Course sand and experiment number 1, influent concentration 5 g l^{-1} . Consequently, MS7-200u refers to Medium Sand experiment number 7, influent concentration 200. In all cases, u refers to upward flow.

3.1. Column apparatus

Column tests are commonly conducted to investigate contaminant migration through soils. The usual test method for a leaching column is to establish steady-state

flow of water through a soil column, and then change the fluid in the influent reservoir to a test solution with a known concentration (e.g., [32]). The effluent concentration is measured at various time intervals by collecting fluid samples at the column exit which are analysed for solute concentration. The resulting solute breakthrough curve is then analysed to provide soil and transport parameters. This approach provides average estimates of the transport parameters for the test soil treated as a single unit within the column, but does not include any variations in the parameters along the length of the column, due to soil structure and packing. By collecting the effluent at the column exit, any additional dispersion caused by the apparatus is included in the determined parameters.

To improve the accuracy of the soil parameter estimates for the displacement experiments, a laboratory column was designed to enable solute concentration and pore pressure to be measured at various locations within the soil. This testing approach minimised errors in the parameter estimates due to both apparatus-induced dispersion and variations in the soil packing with depth. The column was designed to develop a one-dimensional flow regime, minimising side-wall and end effects on the shape of the solute front.

The laboratory column apparatus consisted of an acrylic column with a detachable base and piston top cap. The internal diameter of the column was 80 mm, and the packed soil length was ≈ 435 mm. Instrumentation fixtures were positioned along the length of the column for the pressure and concentration measuring devices. A schematic diagram providing the column dimensions and fixture locations is shown in Fig. 1. Pressure transducers and conductivity probes were located at levels L1–L5, and an additional conductivity probe was located at level L6. The packed soil regions between successive instrumentation levels were labelled from region I–IV, where region I was between levels L1 and L2, and region IV was between levels L4 and L5.

At each end of the column, a ring holder covered with two layers of 0.5 mm thick geofabric was used to contain the soil. Geofabric was chosen in preference to, for example, scintered metal plates after initial experiments showed that a more uniform solute front resulted.

The influent was supplied to the column in different ways depending on the type of test being conducted. For constant head tests, the influent was supplied to the column from an overflow vessel. The overflow vessel was continually refreshed by pumping influent into the vessel from a reservoir.

During the constant head tests the effluent flow rate was found to vary significantly when the influent concentration was high, which complicated the analysis of the results, particularly determination of the hydrodynamic dispersion coefficient, since this parameter depends on the pore fluid flow rate.

During the constant flow rate tests the influent was supplied to the column from a vessel that was manually raised or lowered to maintain a constant flow rate into the column.

For all experiments the effluent line was fixed in position, and the effluent collected in a container. The weight of the effluent container was measured automatically and recorded at regular time intervals. A hanging load frame was used to restrict vertical movement of the top cap during the displacement experiments.

3.2. Instrumentation

The instrumentation consisted of soil and tube conductivity probes and temperature sensors for determining solute concentration, and pressure transducers to measure pore pressures in the soil matrix. The effluent flow rate was measured using either an electronic balance or a load cell. Data were collected automatically at regular intervals using a data acquisition system.

3.2.1. Concentration measurement

Laboratory-scale 4-pin conductivity probes were used. These were subject to extensive development and testing [29] to ensure their reliability over the range of salt concentrations used in the laboratory experiments.

The column was instrumented with conductivity probes located at the edge, inner and middle regions of the column as shown in Fig. 2. Edge, inner and middle probes were located at the base of the column (level L1) to check the uniformity of the influent front as it passed through the base porous plate into the soil. Three probes were also located at levels L2 and L5, to investigate the propagation or development of nonuniform flow through the column.

Data from L6 were used to indicate the degree of apparatus-induced dispersion occurring between the

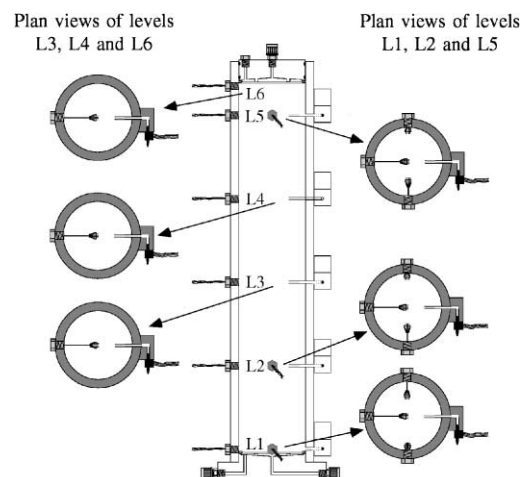


Fig. 2. Diagram of the probe positioning within the column.

upper soil surface plate below the porous plate and the effluent tube probe. Additionally, in the constant flow rate displacement experiments, the data from L6 was used as a measured effluent boundary condition in the numerical model.

3.2.2. Temperature measurements

The fluid temperature was measured using a temperature sensor located in the effluent fluid line. The sensor used was an LM35 precision centigrade temperature sensor. The temperature measurement was used to correct the fluid conductivity measurements for temperature variations as described by [12].

3.2.3. Pressure measurements

Differential pressure transducers, having a pressure range of 0–34.5 kPa, were used to measure the pore pressures within the column. Differential pressure transducers were used because they provided more stable readings than the equivalent gauge transducers at the low pressures developed in the column experiments. All of the column experiments were conducted using atmospheric pressure as the reference pressure on the second port.

The transducer attachments were located along the length of the column in the same horizontal plane as the soil probes at levels L1–L5 (Fig. 2). This setup provided pore pressure and breakthrough curves at five locations within the column. The pore pressure readings were measured in the inner region of the column removing any possible influence of side wall flow variations. The probes were calibrated in-situ over the full experimental range before each test was conducted.

3.2.4. Flow rate load cell

The effluent flow rate from the laboratory column was determined from measurements of the cumulative effluent mass and the effluent concentration. For the constant head displacements conducted on coarse sand (test series I), a cantilever load cell was used to measure the effluent mass.

To improve the accuracy of the remaining constant flow rate experiments (test series II to IV), an HF6000 electronic balance manufactured by A&D Company Ltd. was used to measure the mass of the effluent vessel.

3.3. Materials

3.3.1. Soils

Two grades of sand, produced by Cook Industrial Minerals, were tested in the laboratory column experiments. The particle size distributions of the coarse and medium sands are shown in Fig. 3, and the properties of the soils are given in Table 2. All soil tests were conducted in accordance with Australian Standard AS1289 [25].

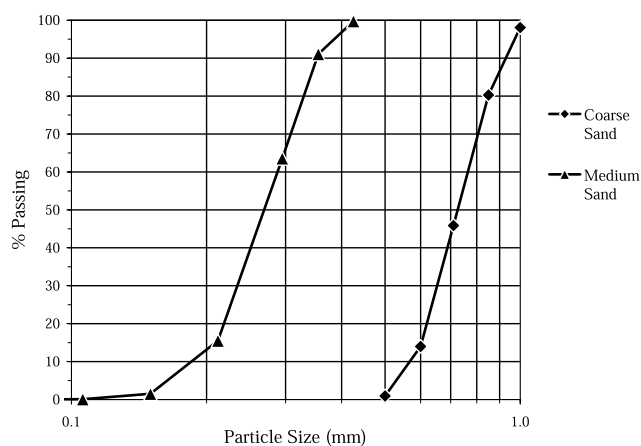


Fig. 3. Particle size distribution curves for coarse and medium sands.

Table 2
Soil properties of the coarse and medium sand

Property	Coarse sand	Medium sand
Median diameter, d_{50} (mm)	0.73	0.27
Effective grain size, d_{10} (mm)	0.57	0.19
Specific gravity	2.65	2.66
Maximum porosity	0.405	0.431
Minimum porosity	0.339	0.357
Effective molecular diffusion coefficient at 20 °C ($\text{m}^2 \text{s}^{-1}$)	1.07×10^{-9}	0.89×10^{-9}

Coarse-grained soil experiments were conducted to investigate the effect of concentration on solute transport when advection was the dominant transport mechanism and mechanical dispersion was the dominant spreading mechanism. Because of the similar grain sizes used, the coarse and medium sand experiments were also conducted so that the results could be compared to the experimental results obtained by [9].

Displacement experiments with high grain Péclet numbers ($\gg 300$) were conducted in the coarse sand to investigate the spreading of the solute front when mechanical dispersion was the dominant spreading mechanism. A greater range of flow rates were used for the medium sand tests to allow investigation of the regimes where mechanical dispersion (high flow rates) or molecular diffusion (low flow rates) would dominate.

3.3.2. Influent solutions

The influent used in the column experiments was sodium chloride (NaCl) solution of varying concentration, within the range 5–200 g l^{-1} (influent ω in the range 0.005–0.1771).

Tabulated density and viscosity values for NaCl solutions at a range of concentrations are readily available [30].

3.4. Column and sample preparation

Four series of displacement experiments were conducted using the coarse-grained soils. Prior to packing the column, the base porous plate, pressure transducers and soil probes were fixed in position and the column was filled with deionised water. To ensure complete saturation of the soil, the column was packed under wet conditions by adding sand slowly to the column and removing the excess water through the base fluid line. The column was vibrated during packing to minimise the soil porosity and prevent rearrangement of the soil grains during the displacement experiments.

The column was packed with soil to just cover the L6 conductivity probe resulting in a soil column of ≈ 440 mm in length. The upper porous plate and top cap were then inserted into the column ensuring that any trapped air was removed. The top cap was loaded via the load frame to a pressure of 10 kPa to prevent swelling or uplift of the soil during the displacement experiments. The influent and effluent lines, vessels and effluent probes were attached and setup for either the constant head or constant flow rate displacement experiments. The column was flushed with at least five pore volumes of deionised water before commencing the displacement experiments.

3.5. Experimental procedure

Two different flow conditions were tested in the laboratory column apparatus by maintaining either a constant influent head or a constant influent flow rate.

The constant head experiments were conducted by maintaining the influent fluid supply at a constant head level throughout the duration of the experiment, using an overflow vessel supplied from the influent reservoir. Before commencing a displacement test the overflow vessel was fixed at the required height and filled with the selected NaCl influent solution. The base of the column was then flushed with the influent solution by opening the waste lines at the column base.

Data logging began with the effluent and waste fluid lines closed, and the influent fluid line open. The initial instrument readings gave the initial pore fluid concentration and hydrostatic pressure distribution within the column. The effluent line was then opened to commence the displacement experiment. The experiment was terminated when the effluent tube probes indicated that complete breakthrough of the influent solution had occurred. This procedure was then repeated using deionised water as the influent solution to flush the column.

The constant flow rate tests were conducted using a similar procedure to the constant head experiments. More details are available elsewhere [2,3].

3.6. Typical breakthrough curves

Typical solute breakthrough curves for three coarse sand tests (CS1-5u, CS1-50u and CS1-200u) are given in Fig. 4. The influent concentrations in the three tests were 5, 50 and 200 g l^{-1} , respectively. The breakthrough curves indicate that the flow was uniform across the majority of the column, however there was a slight lag at the walls. The degree of nonuniformity reduced with increasing influent concentration due to density stabilisation of the influent front.

In the 5 g l^{-1} test (CS1-5u), the effluent tube indicated that significantly more spreading had occurred in the soil than was evident from the L6 middle probe. The additional spreading in the effluent probes was likely caused by side-wall lag. The effluent concentration was effectively an average concentration of the fluid exiting from the entire cross-sectional area of the column. As the solute front exited, the side-wall lag reduced the average effluent concentration and increased the length of time over which breakthrough was occurring,

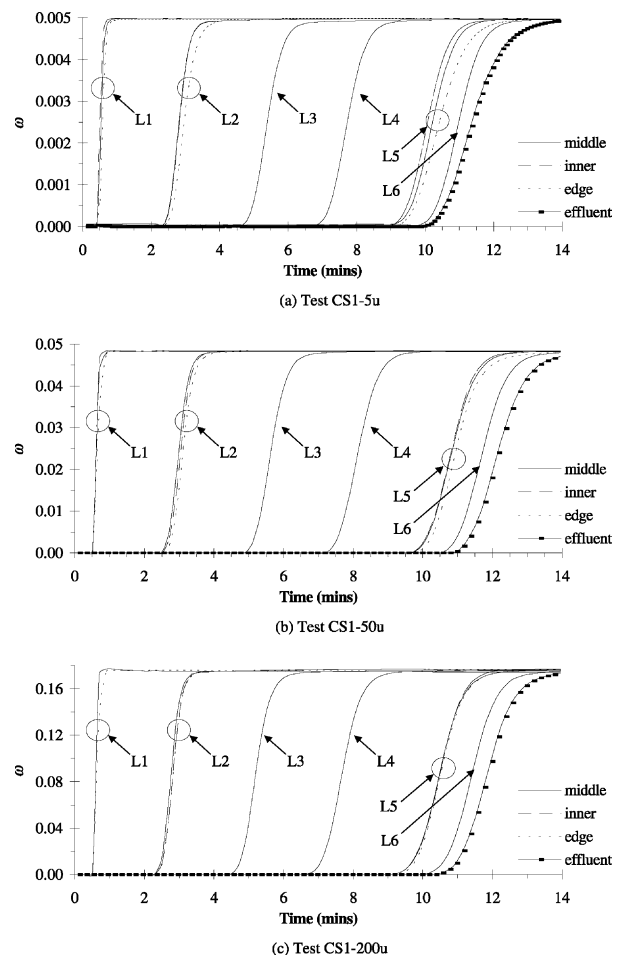


Fig. 4. Typical breakthrough curves showing the degree of nonuniformity in flow within the column. Test (a) CS1-5u, (b) CS1-50u, (c) CS1-200u.

resulting in a more dispersed effluent breakthrough curve. The breakthrough curves for the soil probe at L6 and the effluent tube in the 200 g l⁻¹ test (CS1-200u) show a similar degree of spreading, indicating that apparatus induced dispersion, in the absence of side-wall lag, was not significant for the column apparatus.

The results of the CS1 tests illustrate the advantage of using both tube and soil probes. If a soil probe is inserted at the soil exit and a tube probe is connected to the effluent line, a comparison of the corresponding breakthrough curves for a solute front can indicate if there is significant nonuniform flow occurring within the soil column, or apparatus-induced dispersion.

The breakthrough curves for all of the soil and tube probes were logged throughout each displacement experiment to ensure that the flow was uniform. Side-wall lag was apparent in the majority of low concentration experiments, however the effect was confined to a limited region. For the analysis of the breakthrough curves only the data from the middle probes was used.

4. Data analysis

The procedure used to analyse the experimental data, so as to obtain parameter estimates, is described in detail elsewhere [27], so only brief details will be given here.

Standard finite-difference approaches [4,5,20] were used to solve the governing equations (1)–(6). The model was tested against known solutions to confirm the accuracy of computed results [1]. The nonlinear least-squares fitting approach of [16]—as implemented in the optimisation programme following [21]—was used to determine parameter values from the experimental data. In addition to optimal parameter estimates, this approach gave approximate confidence intervals.

4.1. Parameter estimation procedure

Numerical simulation curves were fitted to the solute breakthrough curves and pressure curves obtained at levels L2–L5 to obtain average parameter estimates for the soil in regions I–IV. The soil parameters determined were the soil porosity, intrinsic permeability, and a dispersion parameter (either the longitudinal dispersivity or the hydrodynamic dispersion coefficient). The flow rate varied significantly during the constant head (CS1–CS4) tests at higher influent concentrations. Therefore, the longitudinal dispersivity was the spreading parameter determined for the constant head tests because, by definition, it is independent of the seepage velocity whereas the hydrodynamic dispersion coefficient is a function of the seepage velocity. When determining the longitudinal dispersivity it was assumed that the mechanical dispersion coefficient was linearly dependent on the seepage velocity, as follows:

$$D_h = D_d^* + a_L|u|, \quad (13)$$

where a_L is the longitudinal dispersivity. This dependence of D_h on u is common, however it has been found that the mechanical dispersion coefficient is more accurately determined by raising the seepage velocity to a power between 1 and 1.2 [6,7,18,22]. Values of D_d^* were determined by [1], as presented in Table 2.

For the constant flow rate displacements in which the seepage velocity remained constant, the hydrodynamic dispersion coefficient was determined, rather than the longitudinal dispersivity. It was preferable to determine the hydrodynamic dispersion coefficient as it is a single parameter quantifying the entire spreading of a solute front due to the combined effects of molecular diffusion and mechanical dispersion. It is reasonably approximated as a constant if the seepage velocity is constant.

When analysing the results from each displacement experiment, initial guesses for the soil parameters in the four soil regions (regions I–IV) were selected. Values for the soil porosity and spreading parameter (either the longitudinal dispersivity or hydrodynamic dispersion coefficient) in the lowest soil region (region I) were then determined using the optimisation programme to fit a numerical solute breakthrough curve to the experimental breakthrough curve at level L2 [27]. The best-fit values for the porosity and spreading parameter were completely determined by the shape of the solute breakthrough curve at level L2, the distance between the probes at levels L1 and L2, and the separation of the breakthrough curves between level L1 (entered as a boundary condition) and L2.

Once the soil porosity and spreading parameter values for region I had been determined, the intrinsic permeability of region I was determined by fitting a numerical pressure curve to the experimental pressure curve at level L2. Using these values, the porosity and spreading parameter for region II were then determined by fitting a numerical solute breakthrough curve to the experimental curve at level L3. This procedure was repeated, first determining the porosity and spreading parameter, followed by the intrinsic permeability for each of the four soil regions within the column. It should be noted that the permeability value for a soil region was dependent on the porosity entered for that region. It was therefore necessary to determine the porosity of a region prior to determining its intrinsic permeability.

After the soil parameters for each displacement were determined, a numerical simulation of the displacement was conducted using the “classical” form of the coupled transport model, i.e., (3)–(6) with the nonextended forms of (1) and (2). After all of the displacements in each test series had been determined, the variation in the parameter estimates with soil type, seepage velocity and influent concentration was investigated to ascertain the

applicability of classical transport theory to high concentration displacements.

5. Results

In this section, we present detailed results from the experiments described above. In addition, we show results of fitting the classical density-dependent flow and transport model to the experimental data. Subsequently (see Section 6), we will discuss the modifications to the classical model described above.

5.1. Test series I: CS1–CS4

The first series of 12 experiments was conducted in coarse sand, with a constant influent head level maintained for each displacement. Two different influent head levels were selected for the displacement tests to investigate high concentration displacements at a fast ($\gg 15 \text{ mm min}^{-1}$) and slow ($\approx 3 \text{ mm min}^{-1}$) seepage velocity. At each influent head level, displacement experiments were conducted with 5, 50 and 200 g l^{-1} influent solutions, and two repeat tests were conducted at the highest influent head level to check the repeatability of the parameter estimates.

5.1.1. Experimental and numerical simulation results

Tests CS1-5u, CS1-50u and CS1-200u were conducted at the highest influent head level. The CS1 solute breakthrough curves from the 12 soil probes and the effluent tube probe are shown in Fig. 4. The breakthrough curves for the 5 g l^{-1} displacement indicate that the flow was slightly nonuniform. This was apparent as the edge probe breakthrough curves lagged behind the middle and inner probe curves at levels L2 and L5 due to side-wall lag.

As the influent solution concentration increased the flow became more uniform due to the stabilising effect of the higher density and viscosity salt solution displacing the lower density and viscosity pore water. This stabilising effect is illustrated in Fig. 4 by the minimal separation of the level L5 breakthrough curves in the 200 g l^{-1} displacement, compared to the L5 curves in the 5 g l^{-1} displacement.

The experimental and fitted solute breakthrough curves (obtained with classical model), pressure curves and the cumulative effluent volume curves for the CS1 displacements are given in Figs. 5 and 6. The experimental and numerical solute breakthrough curves at levels L2 to L5 showed good agreement however most of the experimental breakthrough curves exhibited a small degree of tailing. There was also good agreement between the experimental and numerical pressure curves, with the shape of the experimental and numerical

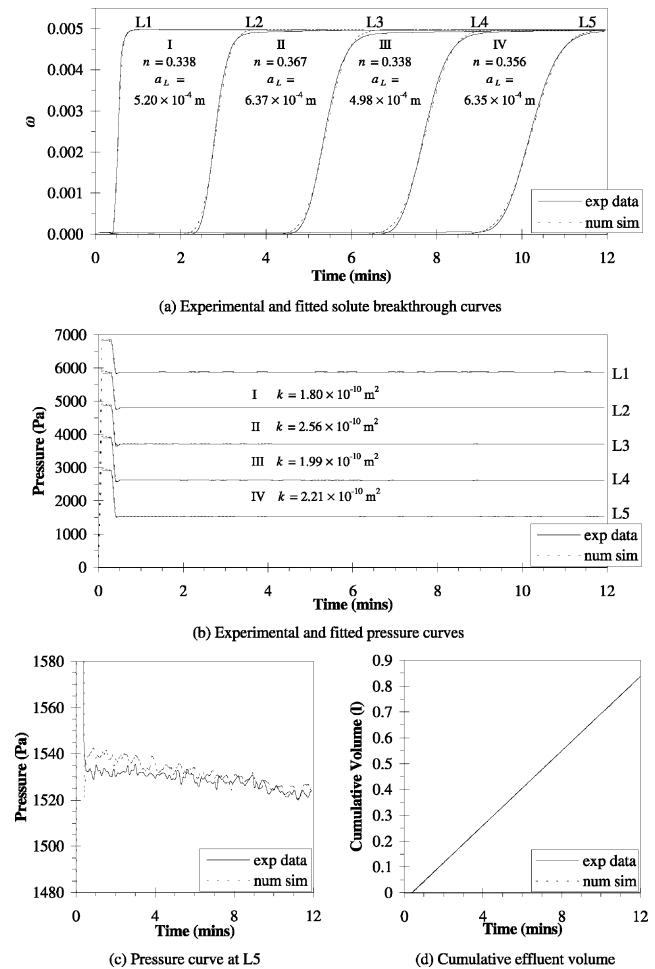
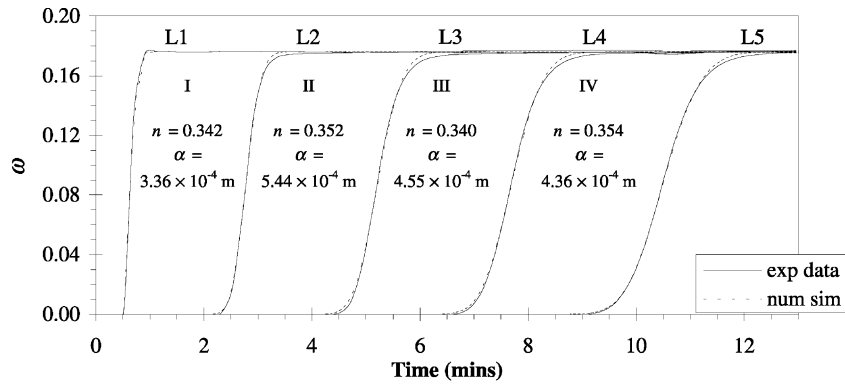


Fig. 5. Experimental data and numerical simulation results for test CS1-5u. (a) Experimental and fitted solute breakthrough curves, (b) experimental and fitted pressure curves, (c) pressure curve at L5, (d) cumulative effluent volume.

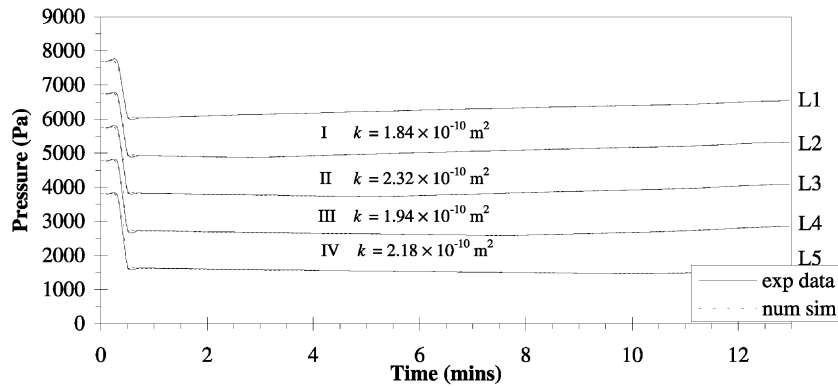
curves matching closely at level L5, shown in Figs. 5c and 6a and c.

The shape of the pressure curves for the higher concentration displacements was quite different to that observed for the low concentration test. Initially the pressure distribution through the column was hydrostatic for all of the displacements. This was followed by a rapid fall in the pressures measured by each transducer when the effluent valve was opened and flow commenced. During the 5 g l^{-1} displacements the pressures reduced slightly, but consistently, throughout the displacement as the 5 g l^{-1} solution moved upwards through the column (Fig. 5b and c). This was due to the slightly greater viscosity of the 5 g l^{-1} influent solution compared to the pore water.

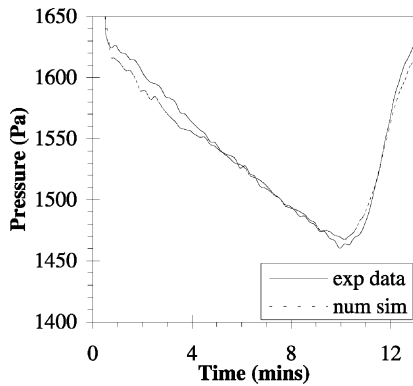
During the high concentration displacements the pressure reduced until the solute front reached the transducer location, then increased as the solute front continued to move through the soil. The reduction and



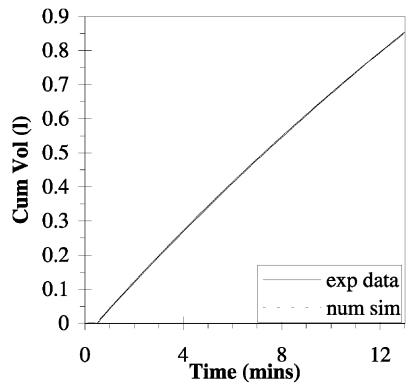
(a) Experimental and fitted solute breakthrough curves



(b) Experimental and fitted pressure curves



(c) Pressure curve at L5



(d) Cumulative effluent volume

Fig. 6. Experimental data and numerical simulation results for test CS1-200u. (a) Experimental and fitted solute breakthrough curves, (b) experimental and fitted pressure curves, (c) pressure curve at L5, (d) cumulative effluent volume.

increase in the measured pressures is very striking in the 200 g l⁻¹ results presented in Fig. 6. See [28] for details.

The experimental and numerical cumulative effluent volume curves for the CS1 displacements are given in Figs. 5d and 6d. The good agreement of the numerical and experimental effluent volume curves indicates that the effluent flux equation used as a fluid boundary condition in the numerical simulations closely matched the experimental flow conditions.

The CS2 and CS3 displacement experiments were repeats of the CS1 experiments (plots of results not

presented). The fitted parameter values obtained from the CS1 to CS3 displacements for region IV are given in Table 3. For region IV the porosity and intrinsic permeability values obtained from the repeat displacements agreed closely with those obtained from the CS1 tests. The longitudinal dispersivity values differed slightly, however this was due to a small difference in flow rate between the tests (Table 5). Good agreement was also obtained between the fitted parameters in the other three soil regions. It was concluded that the experimental setup was providing repeatable and consistent results for analysis.

Table 3
Fitted soil parameters for region IV from the CS1 to CS3 displacements

Influent concentration (g l^{-1})	Test name	Porosity	Longitudinal dispersivity (mm)	Intrinsic permeability ($\times 10^{10} \text{ m}^2$)
5	CS1-5u	0.356	0.635	2.21
	CS2-5u	0.354	0.665	2.23
	CS3-5u	0.360	0.562	2.22
50	CS1-50u	0.356	0.582	2.27
	CS2-50u	0.356	0.554	2.22
	CS3-50u	0.360	0.568	2.23
200	CS1-200u	0.354	0.436	2.18
	CS2-200u	0.358	0.493	2.10
	CS3-200u	0.360	0.457	2.22

The final set of experiments conducted in test series I were the CS4 displacements, which were conducted with a significantly lower influent head level. The solute breakthrough curves for the CS4 experiments from the 12 soil probes and effluent tube probe are shown in Fig. 7. Like the CS1-5u test, the breakthrough curves at levels L2 and L5 in test CS4-5u were separated indi-

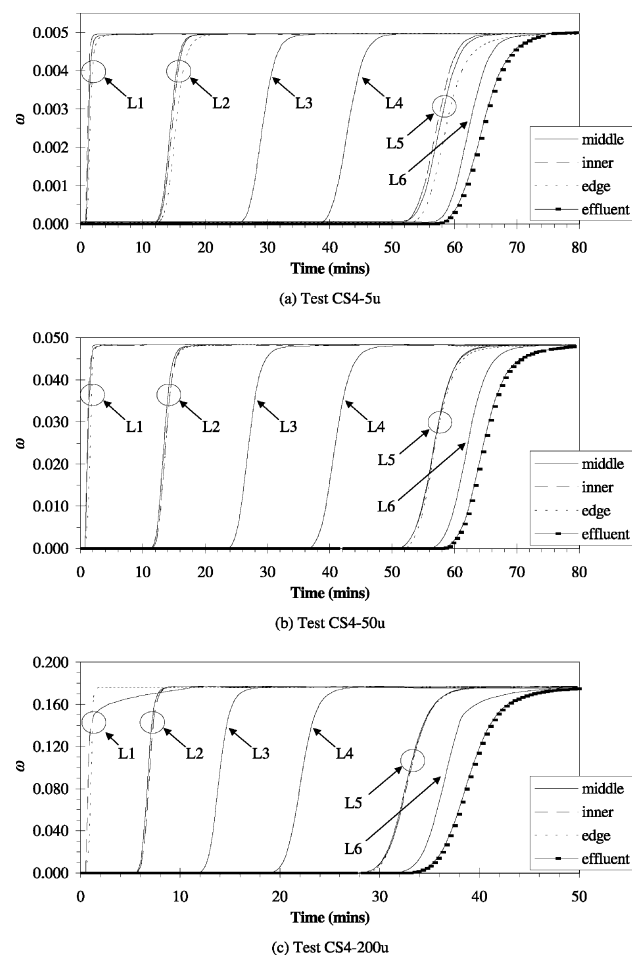


Fig. 7. Solute breakthrough curves for the CS4 experiments. Test (a) CS4-5u, (b) CS4-50u, (c) CS4-200u.

cating that the flow was slightly nonuniform, and sidewall lag was apparent from the edge probe breakthrough curves. At the higher influent concentrations the density and viscosity contrast between the displacing and produced fluid resulted in a stable solute front and nonuniform flow was not apparent.

During the higher concentration displacements the flow rate was found to vary significantly when the influent head level was maintained at a constant height. This variation in flow rate is observable from the solute breakthrough curves for the 200 g l^{-1} displacement (shown in Fig. 7c). For the CS4-200u displacement the flux reduced from 6.14 to 2.47 mm min^{-1} during the displacement (Table 5), a reduction of 60%.

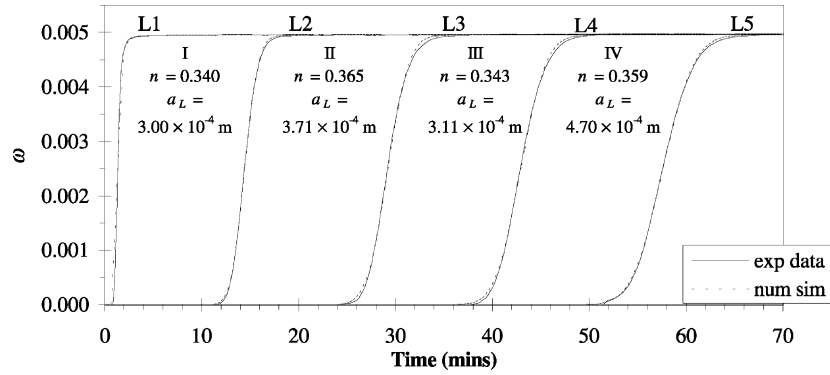
The experimental and numerical solute breakthrough curves, pressure curves and cumulative effluent volume curves are given in Figs. 8 and 9, and a discussion on the fitted parameter values is given in Section 5.2. The experimental and numerical solute breakthrough curves showed good agreement for the three displacement tests, however slight tailing of the experimental results was apparent.

The influent head level for the CS4 experiments was lower than for the CS1–CS3 experiments, resulting in a smaller pressure head change along the length of the column during the CS4 displacements. The resolution of the pressure transducers was too coarse to be able to measure accurately the small pressure head difference between each transducer level, thus the intrinsic permeability values for the CS4 displacements were unable to be determined. For the CS4 numerical simulations, the permeability of each soil region was taken as the average of the fitted permeability values from the CS1 to CS3 tests, given in Table 4. The close-up figures of the level L5 pressure curves (Figs. 8c and 9c) show that the experimental and numerical curves were offset. This difference was caused by a lack of resolution in the pressure transducers, causing inaccurate pressure measurements to be recorded for the low flow rate displacements.

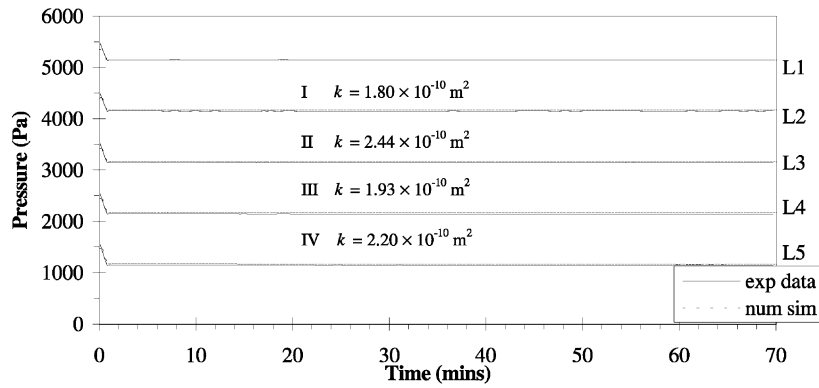
The experimental and numerical cumulative effluent volume curves showed good agreement indicating that the effluent flux polynomial used as the downstream pressure boundary condition accurately represented the experimental conditions. The curvature of the cumulative effluent volume curve for the 200 g l^{-1} displacement, shown in Fig. 9d is a further indication of the flow rate variation that occurred during the high concentration displacement experiments.

5.2. Fitted soil parameters

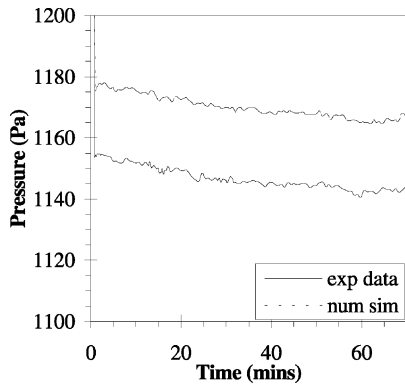
The fitted soil parameters determined from the experimental results were the soil porosity, longitudinal dispersivity and intrinsic permeability. Once all of the displacements from the CS1 to CS4 tests had been



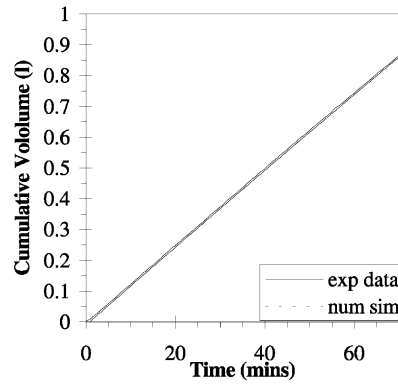
(a) Experimental and fitted solute breakthrough curves



(b) Experimental and fitted pressure curves



(c) Pressure curve at L5



(d) Cumulative effluent volume

Fig. 8. Experimental data and numerical simulation results for test CS4-5u. (a) Experimental and fitted solute breakthrough curves, (b) experimental and fitted pressure curves, (c) pressure curve at L5, (d) cumulative effluent volume.

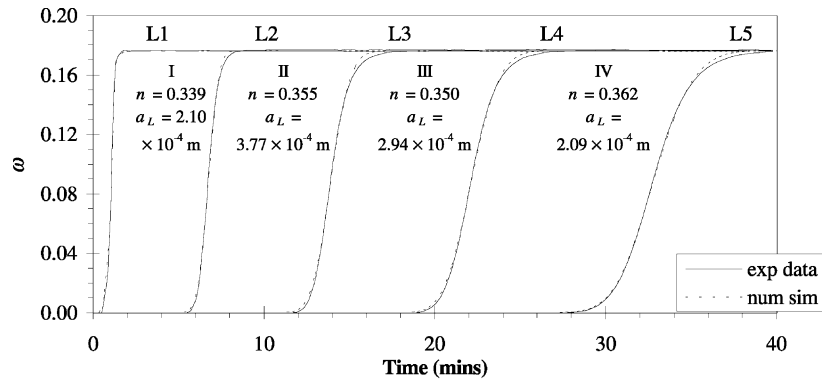
analysed, the variation of parameter values with solute concentration and flow rate was investigated.

5.2.1. Porosity and grain Péclet numbers

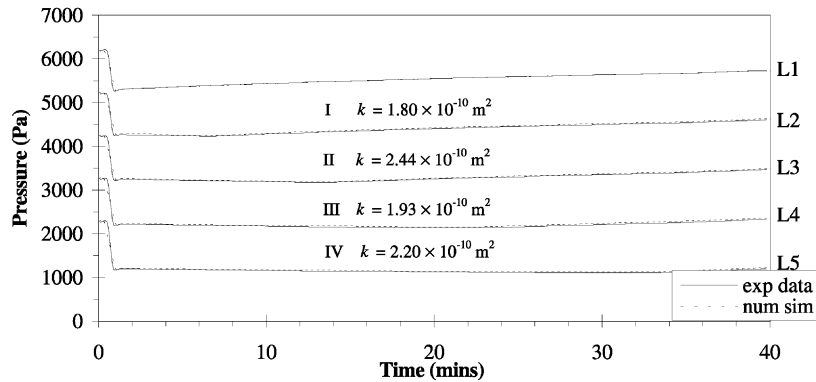
The fitted porosity values from the four soil regions in the CS1–CS4 displacements are shown in Fig. 10. The figure shows the porosity values and trendlines for the four regions. The trendline for regions I and IV indicated that the porosity was not affected by the displacing solution concentration, however the trendline for region II decreased while the trendline for region III increased. It is likely that the porosity variations in regions II and

III were caused by an error in the length estimates of regions II and III used in the numerical program, compared to the actual length. This may have been caused by the level L3 probe being moved during the packing of the column.

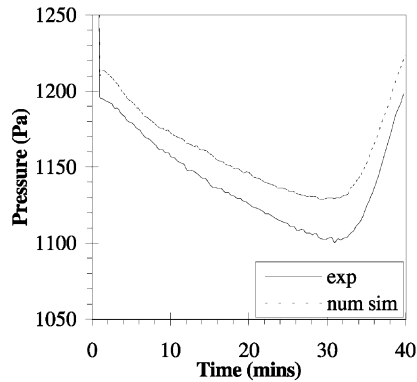
The nonuniform flow mentioned in the experimental results section may have caused some of the variation in the fitted porosity values. In addition to this, the distances between consecutive centre probes used in the numerical simulations were measured before the column was packed. During the packing of the column the probe locations may have shifted, altering the distances



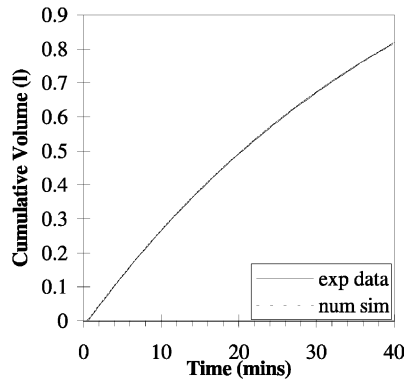
(a) Experimental and fitted solute breakthrough curves



(b) Experimental and fitted pressure curves



(c) Pressure curve at L5



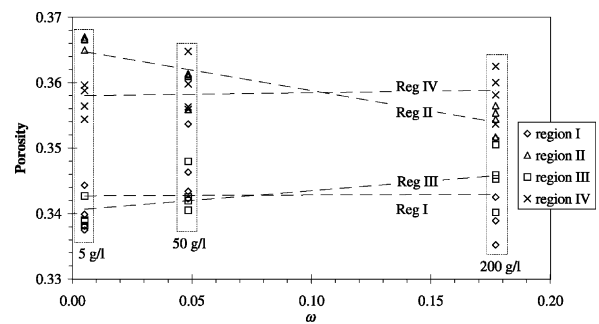
(d) Cumulative effluent volume

Fig. 9. Experimental data and numerical simulation results for test CS4-200u. (a) Experimental and fitted solute breakthrough curves, (b) experimental and fitted pressure curves, (c) pressure curve at L5, (d) cumulative effluent volume.

Table 4
Average fitted permeability values from the CS1–CS3 displacements

Soil region	Intrinsic permeability ($\times 10^{10}$ m ²)
I	1.80
II	2.44
III	1.93
IV	2.20
Average	2.09

between the probes. Any difference between the actual and measured probe separations would result in some variation of the fitted porosity values. It should be noted



(a) Fitted porosity values for the four soil regions at varying influent concentration.

Fig. 10. Fitted porosity values for the CS1–CS4 experiments.

that some of the fitted porosity values, primarily in region I, were below the minimum porosity value of 0.339 presented in Table 2. It is likely that the solute front did not pass through all of the soil around the lower edge of the column because the influent solution was supplied to the column by a central hole in the base plate. Any flow bypassing at the column base would have resulted in slightly lower effective porosity values being determined for region I. The soil at the base of the column was very dense due to the column preparation method, thus the porosity of region I was close to the minimum soil porosity. A reduction in the effective porosity of region I due to flow bypassing would therefore result in fitted porosity values being below the minimum porosity value for coarse sand. Flow bypassing in region I may have also contributed to the slight tailing observed in the experimental results.

The average porosity of the soil in test series I was determined at the end of the test series by measuring the dry mass of soil contained within the known column volume. The average column porosity was measured to be 0.349. The minimum average column porosity from the fitted values for the displacement tests was 0.347 for test CS1-200u, and the maximum average porosity was 0.356 for test CS4-50u, however the majority of average values were between 0.348 and 0.352, in close agreement with the measured porosity of 0.349.

Generally the fitted porosity values were found to be acceptable and agreed with the actual average column porosity. Furthermore, the porosity did not vary significantly with the concentration of the influent solution. This result was a good check on the parameter estimation approach as described in Section 4.1.

The maximum and minimum effluent flux values and grain Péclet numbers for the series I displacements are given in Table 5. The effluent flux remained relatively constant during each low concentration displacement, however, for the higher concentration displacements the effluent flux reduced during each test by as much as 60%.

The grain Péclet number ($ud_{50}D_d^{*-1}$) was determined for each displacement to ensure that mechanical dispersion was the dominant spreading mechanism. The characteristic length, d_{50} , was taken as the median grain diameter, 0.73 mm, and the diffusion coefficient was taken from Table 2. The minimum grain Péclet number determined for the series I displacements was 66 for test CS4-50u, and the other grain Péclet numbers all exceeded 70. This indicated that mechanical dispersion was the dominant spreading mechanism, and the smaller longitudinal dispersivity values determined at the slower flow rates in the CS4 tests were not due to molecular diffusion becoming the dominant spreading mechanism.

5.2.2. Intrinsic permeability

The fitted intrinsic permeability values for the CS1–CS3 displacements are presented in Fig. 11. The intrinsic permeability of regions I and III increased slightly with increasing influent solution concentration whereas the permeability of regions II and IV decreased slightly with increasing concentration. As for the variations in porosity, it is likely that these increasing and decreasing trends resulted from an error in the determination of the distance between consecutive pressure transducers.

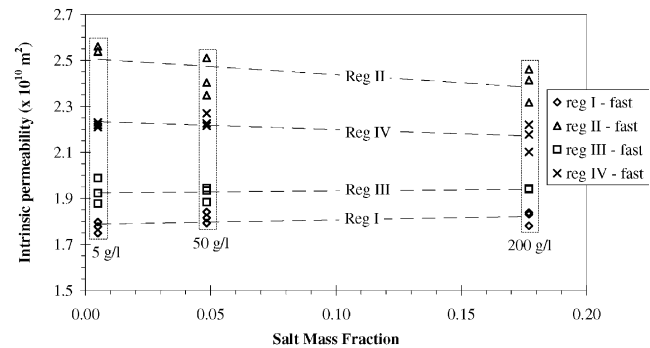


Fig. 11. Fitted intrinsic permeability values for the CS1–CS3 experiments.

Table 5
Minimum and maximum effluent flux values and grain Péclet values for the series I displacements

Test	Maximum effluent flux (mm min ⁻¹)	Minimum effluent flux (mm min ⁻¹)	Maximum grain Péclet number	Minimum grain Péclet number
CS1-5u	14.3	14.3	466	466
CS1-50u	14.1	12.9	459	420
CS1-200u	16.4	11.4	534	371
CS2-5u	13.8	13.8	450	450
CS2-50u	14.4	13.0	469	424
CS2-200u	15.4	10.7	502	349
CS3-5u	13.3	13.3	433	433
CS3-50u	14.0	12.9	456	420
CS3-200u	16.3	12.0	531	391
CS4-5u	2.53	2.41	82	79
CS4-50u	2.90	2.04	94	66
CS4-200u	6.14	2.47	200	80

Table 6
Fitted and calculated permeability values for regions II and III from the CS1 to CS3 200 g l⁻¹ displacements

Test name	Permeability ($\times 10^{10}$ m ²)			
	Region II		Region III	
	Fitted	Darcy's law	Fitted	Darcy's law
CS1-200u	2.32	2.35	1.94	1.93
CS2-200u	2.46	2.47	1.94	1.89
CS3-200u	2.41	2.32	1.94	1.90

The fitted values obtained for the 200 g l⁻¹ displacements were compared to permeability values calculated using Darcy's law, following complete breakthrough of the influent solution. The fitted and calculated permeability values from CS1-200u, CS2-200u and CS3-200u for regions II and III are given in Table 6. The fitted permeability values, obtained by fitting numerical pressure curves to the experimental curves, closely matched the permeability values calculated using the "standard" Darcy's law. These results indicate that the numerical model, which was formulated from the classical transport theory, is accurately modelling Darcy's law at high influent solution concentrations.

Hassanzadeh & Leijnse [11] found that the intrinsic permeability of their porous medium (glass beads with diameters ranging from 0.40 to 0.52 mm) reduced by 15% as the influent solution salt mass fraction was increased from 0.001 to 0.24. Here, however, the intrinsic permeability values did not vary consistently over the influent salt mass fraction range from 0.005 to 0.1771. It was therefore concluded that the intrinsic permeability was not a function of the influent solution concentration.

5.3. Test series II: tests CS5–CS10

The displacement experiments conducted in test series II were conducted in coarse sand, like the series I displacements. A constant flow rate was maintained throughout each displacement. Six flow rates were used for the displacements, with the CS5 displacements being conducted at the fastest flow rate and the CS10 displacement at the slowest flow rate. At each flow rate one or more displacements were conducted using influent solution concentrations in the range from 5 to 200 g l⁻¹.

5.3.1. Experimental and numerical simulation results

Tests CS5-5u and CS5-200u were conducted at the fastest flow rate, with an average flux of 15.6 mm min⁻¹ for CS5-5u, and 15.5 mm min⁻¹ for CS5-200u. The experimental and fitted solute breakthrough curves, pressure curves and effluent flux curves are given in Figs. 12 and 13. The fitted solute breakthrough curves for the 5 and 200 g l⁻¹ displacements showed good agreement

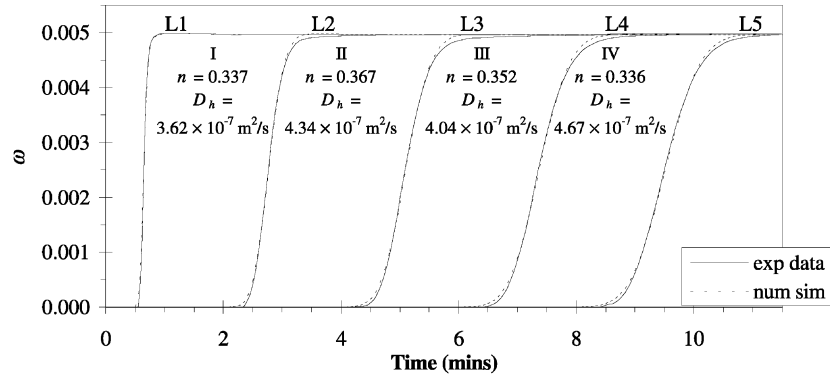
with the experimental results, however slight tailing of the experimental curves was apparent. The experimental and fitted pressure curves also showed good agreement for both the 5 and 200 g l⁻¹ displacements, highlighted by the closely matched experimental and numerical pressure curves at level L5, shown in Figs. 12c and 13c. The measured experimental effluent flux was used as the effluent boundary condition for the fluid in the numerical model. A comparison of the experimental effluent flux and the effluent flux calculated during the numerical simulation for a point just inside the effluent boundary is given in Figs. 12d and 13d for the 5 and 200 g l⁻¹ displacements, respectively. The figures indicate that the effluent fluid boundary condition closely matched the effluent flux data measured in the experiments, thus the experimental flow conditions were accurately modelled by the numerical simulations.

Figs. 12b and 13b present the fluid pressures at the five transducer locations. The initial pressures were hydrostatic, reducing as the experiment commenced. Once flow had started the supply vessel was lowered to maintain a constant flow rate (Section 3.1), but in both the 5 and 200 g l⁻¹ displacements the vessel was lowered slightly more than necessary and had to be raised almost immediately. This resulted in a dip in the pressure at the start of both displacements, observable in Figs. 12c and 13c.

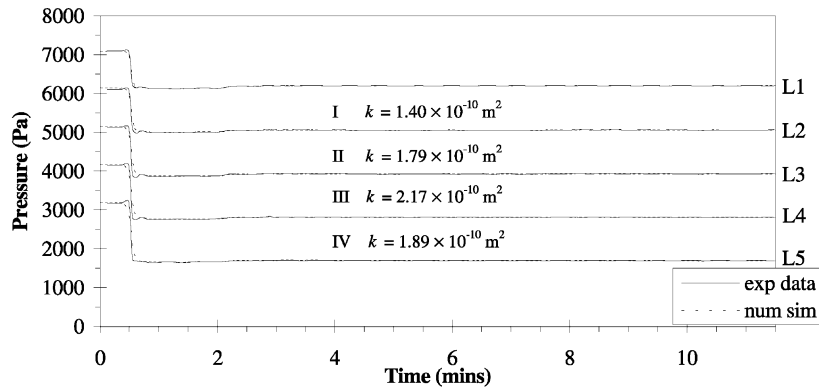
For the low concentration test, CS5-5u, the pressures measured at the five locations within the column remained constant throughout the experiment, once the flow rate was approximately constant. For the high concentration displacement, once the flow rate was approximately constant, the pressures measured within the column remained constant until the solute front reached the location at which the pressure was being measured. As the solute front passed this location and continued moving upwards through the column an increasing fluid pressure was measured. The level L5 pressure curve for the 200 g l⁻¹ displacement is shown in Fig. 13c. Once a relatively constant flow rate had been established within the column, the pressure measured at level L5 remained constant until ≈ 9 min had passed, after which time the pressure rapidly increased. Fig. 13a indicates that the solute front passed the level L5 transducers at 9 min, as expected from the L5 pressure results.

The CS6 displacements were the second set of tests conducted in series II. Five experiments were conducted with influent concentrations of 5, 50, 100, 150 and 200 g l⁻¹ (CS6-5u to CS6-200u, respectively). The nominal flow rate selected for the CS6 displacements was approximately 40% of the flow rate maintained during the CS5 displacements. The average effluent flux values for the CS6 tests are given in Table 7.

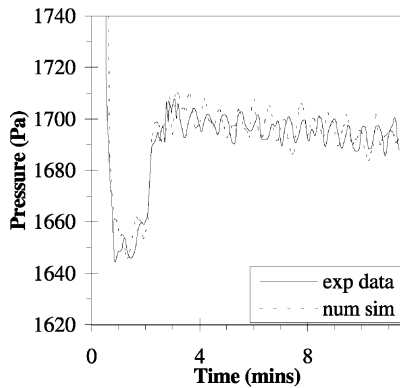
Only the results for the CS6-100u experiment are presented (see Fig. 14). The fitted pressure curves showed excellent agreement with the measured pressure



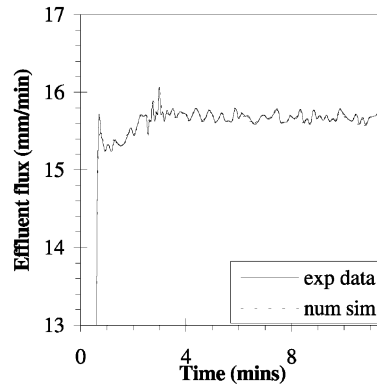
(a) Experimental and fitted solute breakthrough curves



(b) Experimental and fitted pressure curves



(c) Pressure curve at L5



(d) Effluent flux

Fig. 12. Experimental and fitted results for test CS5-5u. (a) Experimental and fitted solute breakthrough curves, (b) experimental and fitted pressure curves, (c) pressure curve at L5, (d) effluent flux.

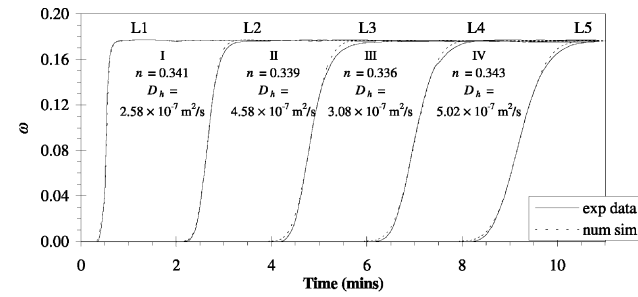
curves for all of the CS6 displacements. The pressure curves in the CS6 experiments were similar in shape to the CS5 pressure curves.

As for the CS5 experiments, the comparison of the measured experimental effluent flux and the effluent flux calculated during the numerical simulation for the CS6 displacements (e.g., Fig. 14d), showed good agreement.

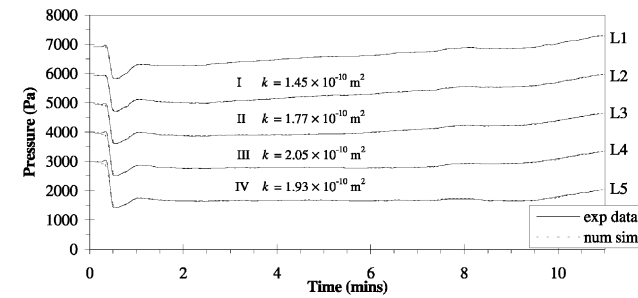
A further seven displacements were conducted in test series II at four different selected flow rates, in the CS7–CS10 tests. Two displacements were conducted in the CS7, CS8 and CS9 test sets with influent solutions

having concentrations of 5 and 200 g l⁻¹. The final test in set CS10 was a 5 g l⁻¹ displacement. The selected flow rates for the displacements in test sets CS7–CS9 were ≈50% of the flow rate from the previous test set, and the flow rate in the CS10 displacement was ≈25% of the flow rate in test set 9 (Table 7).

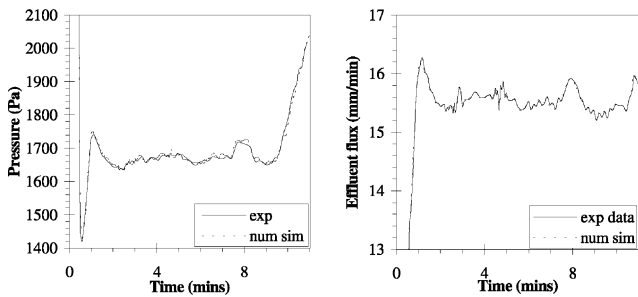
The comparison of the experimental and fitted solute breakthrough curves and effluent flux curves for the CS7–CS10 displacements also showed similar trends to the CS5 and CS6 experiments. In particular, good agreement was obtained between the experimental and



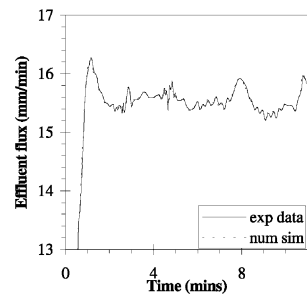
(a) Experimental and fitted solute breakthrough curves



(b) Experimental and fitted pressure curves



(c) Pressure curve at L5



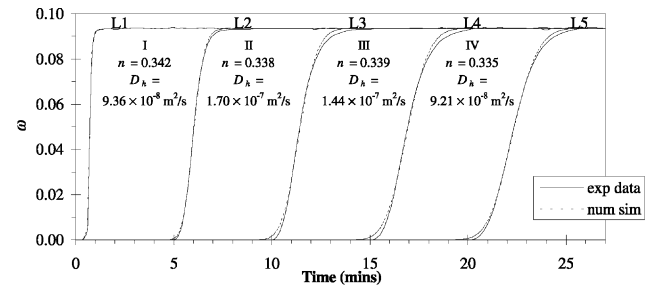
(d) Effluent flux

Fig. 13. Experimental and fitted results for test CS5-200u. (a) Experimental and fitted solute breakthrough curves, (b) experimental and fitted pressure curves, (c) pressure curve at L5, (d) effluent flux.

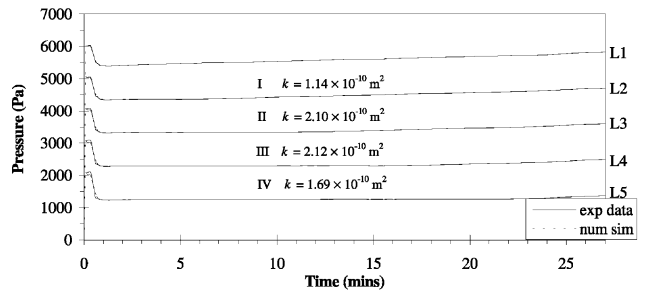
Table 7
Average effluent fluxes and grain Péclet numbers for the CS5–CS10 experiments

Test name	Average effluent flux (mm min ⁻¹)	Grain Péclet number
CS5-5u	15.6	523
CS5-200u	15.5	520
CS6-5u	5.98	201
CS6-50u	6.14	206
CS6-100u	6.23	209
CS6-150u	6.14	206
CS6-200u	6.21	208
CS7-5u	3.05	102
CS7-200u	3.08	103
CS8-5u	1.65	55
CS8-200u	1.64	55
CS9-5u	0.79	26
CS9-200u	0.83	28
CS10-5u	0.20	7

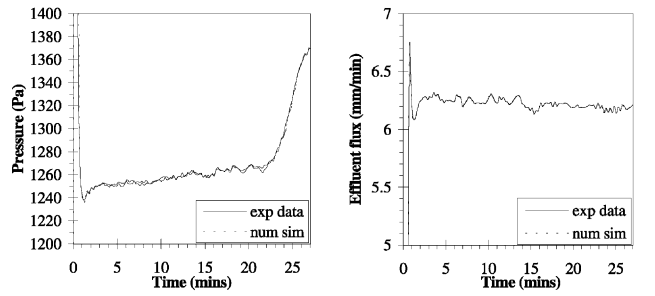
numerical solute breakthrough curves, although slight tailing of the experimental breakthrough curves was apparent in all of the displacements, irrespective of the



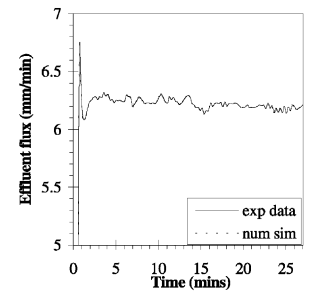
(a) Experimental and fitted solute breakthrough curves



(b) Experimental and fitted pressure curves



(c) Pressure curve at L5



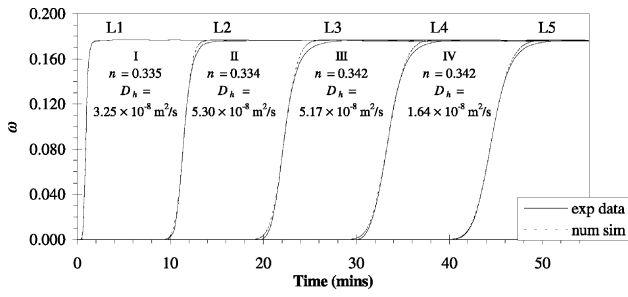
(d) Effluent flux

Fig. 14. Experimental and fitted results for test CS6-100u. (a) Experimental and fitted solute breakthrough curves, (b) experimental and fitted pressure curves, (c) pressure curve at L5, (d) effluent flux.

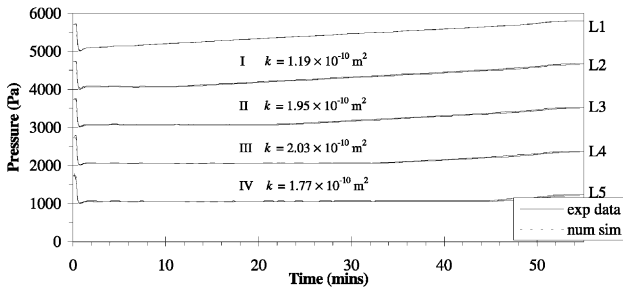
flow rate. Typical results are presented for one experiment, CS7-200u, in Fig. 15.

The flow rates used in the CS7–CS10 experiments were significantly slower than the flow rates used in the CS5 and CS6 experiments, resulting in a small change in pressure head along the length of the column during the CS7–CS10 displacements. For these slower displacements, the resolution of the pressure transducers was too coarse for accurate values of the pressure head differential between transducers to be determined, and so estimates of the intrinsic permeability values were unable to be determined. A similar situation was also encountered in the CS4 displacements. For the CS7–CS10 displacements the intrinsic permeability values for the four soil regions were taken as the average of those obtained from the CS5 and CS6 tests, for which the intrinsic permeability values were accurately determined.

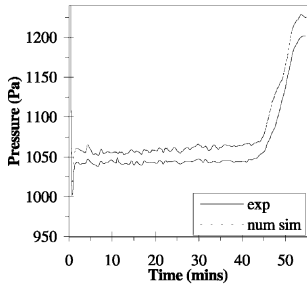
The numerical pressure curves were not fitted to the experimental pressure curves for the CS7–CS10 dis-



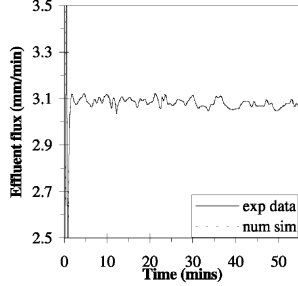
(a) Experimental and fitted solute breakthrough curves



(b) Experimental and fitted pressure curves



(c) Pressure curve at L5



(d) Effluent flux

Fig. 15. Experimental and fitted results for test CS7-200u. (a) Experimental and fitted solute breakthrough curves, (b) experimental and fitted pressure curves, (c) pressure curve at L5, (d) effluent flux.

placements resulting in an offset between the curves (e.g., Fig. 15c). This difference was also due to the lack of resolution of the pressure transducers, causing inaccurate pressure measurements for low flow rate displacements.

5.3.2. Fitted soil parameters

The fitted soil parameters determined from the experimental results for the series II displacements were the soil porosity, hydrodynamic dispersion coefficient and intrinsic permeability. The fitted parameters from the CS5 to CS10 tests were compared so that the variation of parameter values with solute concentration and flow rate could be investigated.

5.3.2.1. Porosity. The fitted porosity values determined for soil regions I–IV for the CS5–CS10 tests are presented in Fig. 16.

Within each soil region, the fitted porosity values were generally spread over a larger range of values at the

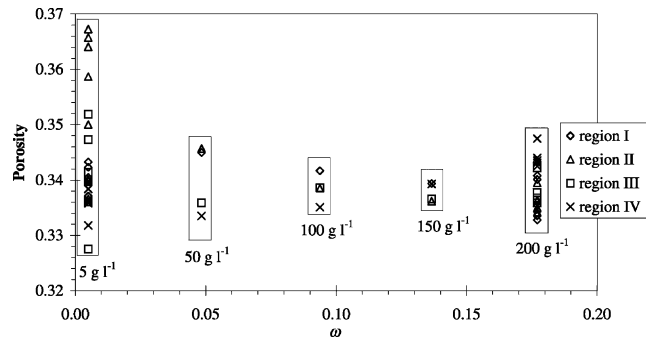


Fig. 16. Fitted porosity values for the CS5–CS10 experiments.

lowest influent concentration of 5 g l⁻¹ than at the highest concentration of 200 g l⁻¹. This was due to the development of nonuniform flow within the column, which would have been stabilised more rapidly for the higher concentration displacements. The fitted porosity values for soil regions I and II showed a slight decreasing trend with increasing concentration, whereas the region III porosity values remained relatively constant, and the region IV values increased slightly with increasing concentration. Although trends were apparent in each soil region, the trends were slight and not consistent.

Following the completion of the series II experiments, the average porosity of the soil was determined independently by measuring the dry mass of soil contained within the known column volume. The measured average soil porosity for the packed column was 0.339. This indicated that the soil in the column was densely packed at the maximum dry density for coarse sand. The average fitted porosity values for the four soil regions from all of the displacement experiments are given in Table 8.

Generally, the fitted porosity values for the four soil regions were found to be acceptable and in good agreement with the actual column porosity.

5.3.2.2. Hydrodynamic dispersion coefficient. The fitted hydrodynamic dispersion coefficients determined for the 5 and 200 g l⁻¹ displacements in test series II are presented in Fig. 21. The figure presents the fitted hydrodynamic dispersion coefficients graphed against the average seepage velocity from the 5 and 200 g l⁻¹ displacements for the four soil regions. Included in this plot is a curve representing the hydrodynamic dispersion equation (13), in which the mechanical dispersion is assumed to be a linear function of the seepage velocity. For this equation, the longitudinal dispersivity was equal to 0.5 mm, to fit the curve to the hydrodynamic dispersion coefficients determined at the fastest flux of 15.5 mm min⁻¹. The salient feature of Fig. 21 is that the shape of the assumed curve determining the

Table 8
Average porosity values for the four soil region in test series II

Soil region	Fitted soil porosity
I	0.339
II	0.346
III	0.339
IV	0.339
Average	0.341

hydrodynamic dispersion coefficient did not fit the experimental results. In particular, the correct equation for hydrodynamic dispersion coefficient should produce a steeper curve to adequately fit the experimental data, thus must be a nonlinear function of the seepage velocity. The inadequacy of the hydrodynamic dispersion equation was also apparent from the series I displacements, in which the longitudinal dispersivity was found to vary with the seepage velocity (Section 5.2.1). The required modifications of the hydrodynamic dispersion equation are discussed in Section 6.

The results for each soil region revealed that the fitted dispersion coefficients were higher for the low influent solution concentration of 5 g l^{-1} , than for the high influent solution concentration of 200 g l^{-1} . There are two possible explanations for this. First, the flow in the low concentration displacements was found to be slightly nonuniform whereas in the high concentration displacements the flow was uniform. Flow nonuniformity at the low influent solution concentration may have caused more spreading of the solute front, resulting in larger dispersion coefficients. However, the solute breakthrough curves analysed were obtained from the middle probes of the column, and the nonuniform flow region was confined to the edge of the column. Non-uniform flow was therefore unlikely to have caused the disparity in low concentration and high concentration dispersion coefficients.

A more likely explanation for the disparate dispersion coefficients is that the large density, viscosity and concentration gradients were altering the dispersion of the solute front in the high concentration displacements (Section 1). The density, viscosity and concentration gradient across the solute front was significantly greater for the 200 g l^{-1} influent solution than for the 5 g l^{-1} case. Therefore, the lower dispersion coefficients determined for the higher concentration displacements provide experimental evidence that the classical formulation of Fick's law needs to be modified for high concentration displacements.

5.3.2.3. Intrinsic permeability. The fitted intrinsic permeability values for the CS5 and CS6 displacements are presented in Fig. 17. The intrinsic permeability values determined for the four soil regions are presented in

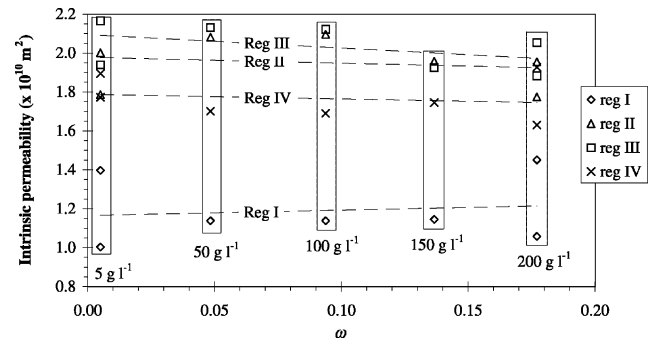


Fig. 17. Fitted intrinsic permeability values for the CS5 and CS6 experiments.

Fig. 17. The trendline for region I showed a slight increase in permeability with increasing influent solution concentration, whereas the trendlines for regions II, III and IV showed a slight decrease. However, the permeability changes indicated by the trendlines were small over the range of concentrations tested, compared to the scatter in the experimental results. The average fitted permeability values from the CS5 and CS6 displacements are given in Table 9. The average permeability from the series II displacements was $1.83 \times 10^{-10} \text{ m}^2$ which was slightly lower than the average permeability from the series I displacements of $2.09 \times 10^{-10} \text{ m}^2$. This difference in permeability was due to a denser packing in the series II displacements, indicated by the higher average porosity in the series I displacements than in the series II displacements.

It was concluded from the inspection of Fig. 17 that the intrinsic permeability of the coarse sand was not affected by the displacing solution concentration.

5.4. Test series III: tests MS1–MS7

The experiments conducted in the third series of tests were constant flow rate displacements, similar to those conducted in test series II. The test soil used in the series III displacements was a medium sand. A finer sand was tested to provide accurate intrinsic permeability values over a wider range of flow rates than was possible with the coarse sand, and to investigate whether the obser-

Table 9
Average fitted permeability values from the CS5 to CS6 displacements

Soil region	Intrinsic permeability ($\times 10^{10} \text{ m}^2$)
I	1.71
II	1.79
III	1.92
IV	1.90
Average	1.83

vations made from the coarse sand displacements were applicable to another grade of soil. Seven flow rates were used during the series III displacements with the fastest average fluid flux being 11.8 mm min^{-1} and the slowest flux being 0.17 mm min^{-1} . A total of 15 displacements were conducted in test series III. The average effluent fluxes and grain Péclet numbers are listed in Table 10.

5.4.1. Experimental and numerical simulation results

Two displacements, MS1-5u and MS1-200u, were conducted at the fastest flow rate using 5 and 200 g l^{-1} influent solutions. The average flux for the tests was 11.8 and 11.7 mm min^{-1} , respectively.

The fitted solute breakthrough curves (only the MS1-200u results are shown, Fig. 18) from the MS1 tests showed good agreement with the experimental curves, however slight tailing of the experimental curves was apparent in both the 5 and 200 g l^{-1} displacements. The fitted pressure curves and experimental pressure curves showed good agreement for the 5 g l^{-1} displacement, however there was a slight variation in shape between the experimental and numerical pressure results for the 200 g l^{-1} displacement. This was due to the sensitivity of the numerical pressure curves to the effluent flux boundary condition under the test conditions of high flow rate and low intrinsic permeability. The experimental pressure curves from the two displacements were similar in shape to those obtained in the series II displacements.

The experimental and numerical effluent flux curves for the MS1 displacements (e.g., Fig. 18d), showed good agreement, indicating that the experimental flow conditions were accurately represented in the numerical simulations. Note that a problem was encountered

Table 10
Average effluent fluxes and grain Péclet numbers for the MS1–MS7 experiments

Test name	Average effluent flux (mm min^{-1})	Grain Péclet number
MS1-5u	11.8	162
MS1-200u	11.7	160
MS2-5u	8.1	111
MS2-50u	7.8	107
MS2-100u	8.1	111
MS2-200u	8.1	111
MS3-5u	5.8	80
MS3-200u	6.1	84
MS4-5u	3.9	53
MS4-200u	4.0	55
MS5-5u	2.0	27
MS5-200u	2.0	27
MS6-5u	0.4	6
MS6-200u	0.4	6
MS7-5u	0.2	2

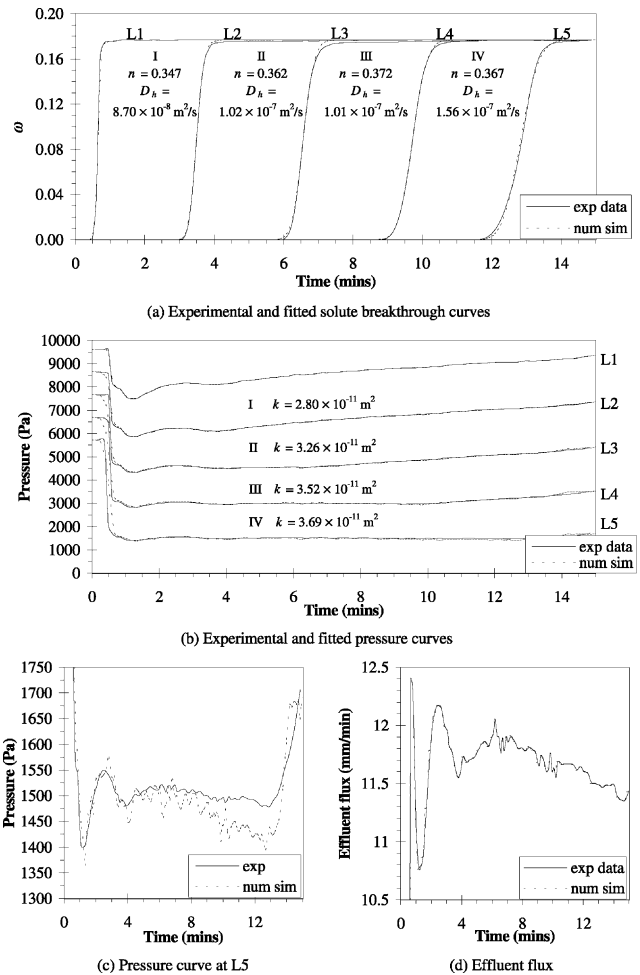


Fig. 18. Experimental and fitted results for test MS1-200u. (a) Experimental and fitted solute breakthrough curves, (b) experimental and fitted pressure, (c) pressure curve at L5, (d) effluent flux.

during test MS1-200u with the manual height control of the influent supply vessel which caused some flow rate variations during the displacement, however the problem was rectified for the subsequent displacements.

In test series III a further 13 displacements were conducted at six different flow rates (test sets MS2–MS7). The experimental and numerical results from these displacements are similar to the MS1 results and are not presented in detail.

The comparison of the measured experimental effluent flux and the effluent flux calculated during the numerical simulation for the MS2–MS7 displacements showed good agreement, indicating that the experimental flow conditions were accurately modelled in the numerical simulations.

5.4.2. Fitted soil parameters

The fitted soil parameters obtained from the analysis of the series III displacements were the soil porosity,

hydrodynamic dispersion coefficient and intrinsic permeability for the four soil regions.

5.4.2.1. *Porosity.* The fitted porosity values for the four soil regions graphed against the displacing solution concentration are presented in Fig. 19.

At the end of the medium sand column experiments the soil in the column was dried and weighed and the average soil porosity was determined. The average porosity of the packed medium sand was 0.369, slightly higher than the minimum porosity for medium sand of 0.357 (Table 2). The average porosity values for the four soil regions are presented in Table 11. The overall column porosity calculated from all of the displacement porosities was 0.357 which was lower than the actual value of 0.369. The average porosities of regions I and IV were below the minimum medium sand porosity of 0.357. This was possibly due to lower than actual porosities being determined for the lower concentration displacements which exhibited side-wall lag, or perhaps a small amount of “dead” pore space. The average fitted porosity values were then calculated for the 200 g l⁻¹ displacements in which the flow was uniform. In this case the overall column porosity was 0.366 which agrees very well with the measured column porosity of 0.369.

5.4.2.2. *Hydrodynamic dispersion coefficients.* The fitted hydrodynamic dispersion coefficients determined for the

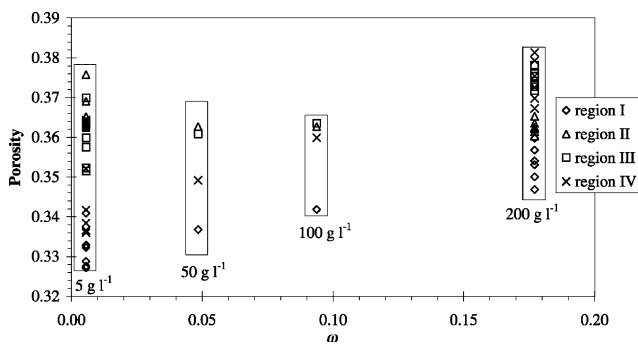


Fig. 19. Fitted porosity values for the MS1–MS7 experiments.

Table 11
Average porosity values for the four soil regions in test series III

Soil region	Average soil porosity	
	All displacements	200 g l ⁻¹ displacements
I	0.341	0.353
II	0.364	0.363
III	0.366	0.375
IV	0.357	0.374
Average	0.357	0.366

5 and 200 g l⁻¹ displacements in test series III are presented in Fig. 22. The hydrodynamic dispersion coefficients determined for the four soil regions are graphed in Fig. 22 against the average seepage velocity of the displacing solution. Included in this plot is a curve representing the hydrodynamic dispersion Eq. (13).

The medium sand dispersion results presented in Fig. 22 show similar features to the results presented in Fig. 21 for the coarse sand displacements conducted in test series II. In particular, Eq. (13) for determining the hydrodynamic dispersion coefficient does not agree with the experimental results obtained from either the low or high concentration displacements. It is apparent from Fig. 22 that the hydrodynamic dispersion equation must produce a steeper curve to fit the experimental data.

Another feature of the medium sand results, also apparent in the coarse sand results (Section 5.2) is that the dispersion coefficients determined for the low concentration displacements were higher than the coefficients determined for the high concentration displacements at the same average flow rate.

5.4.2.3. *Intrinsic permeability.* The fitted intrinsic permeability values determined for the MS1–MS4 displacements are graphed against the influent solution concentration in Fig. 20. In this figure, the intrinsic permeability values for the four soil regions are graphed with trendlines marked for the permeability data from each soil region. The trendlines indicate that the intrinsic permeability of the soil was not affected by the influent solution concentration.

6. Discussion

6.1. Applicability of Darcy’s law

In Section 5, the applicability of Darcy’s law to high concentration displacements was investigated by fitting numerical solutions to the experimental results from the

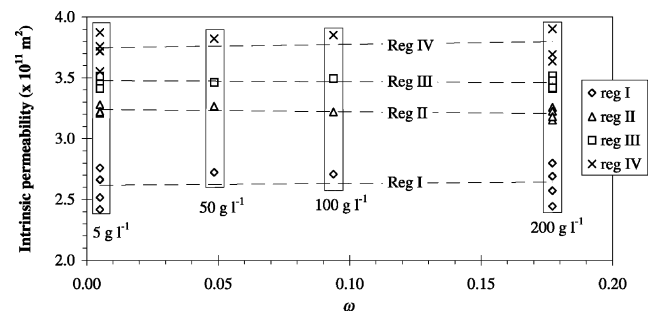


Fig. 20. Fitted intrinsic permeability values for the MS1–MS7 experiments.

low and high concentration displacement experiments. The numerical model was based on the classical density-dependent solute transport theory which was formulated using the classical version of Darcy’s law.

Numerical pressure curves were fitted to the experimental pressure curves from the low and high concentration displacements to obtain fitted intrinsic permeability values for the soil in regions I–IV. The applicability of Darcy’s law to the displacements was then assessed by examining the shapes of the numerical and experimental pressure curves, and by investigating the variation of the fitted intrinsic permeability values with influent solution concentration.

The simulated numerical pressure curves closely matched the shape of the experimental pressure curves for the low and high concentration displacements in both the constant head and constant flow rate tests. This indicated that the classical formulation of Darcy’s law adequately represented the fluid flow processes occurring within the porous medium. This finding agrees with that of [17,31], who reported that osmotically driven flow would normally only be of significance in very low permeability soils.

The fitted intrinsic permeability values from the faster displacements in test series I, II and III were plotted against influent solution concentration for the four soil regions, as shown in Figs. 11, 17 and 20, respectively. These results confirmed the observation that Darcy’s law was applicable to high concentration displacements in coarse-grained soils.

6.2. Hydrodynamic dispersion

The dispersion results from the constant head and constant flow rate displacements indicated that the hydrodynamic dispersion coefficient was a nonlinear function of the seepage velocity (Figs. 21 and 22).

The fitted hydrodynamic dispersion coefficients determined from the constant flow rate displacements in coarse sand (test series II) are presented in Fig. 21.

A nonlinear dispersion equation having the following formulation was fitted to the 5 and 200 g l⁻¹ results using a least-squares method:

$$D_h = D_d^* + a_L |u|^m, \tag{14}$$

The nonlinear dispersion equations fitted to the 5 and 200 g l⁻¹ displacement results are represented by curves shown in Fig. 21. It is apparent from these curves that the dispersion was greater at the lower concentration of 5 g l⁻¹ than at the higher concentration. Previously *m* has been found to lie within the range of 1.0–1.2 (Section 4.1). The exponent from the 5 g l⁻¹ displacements was slightly higher than this range, however the exponent fitted to the 200 g l⁻¹ results was significantly higher than

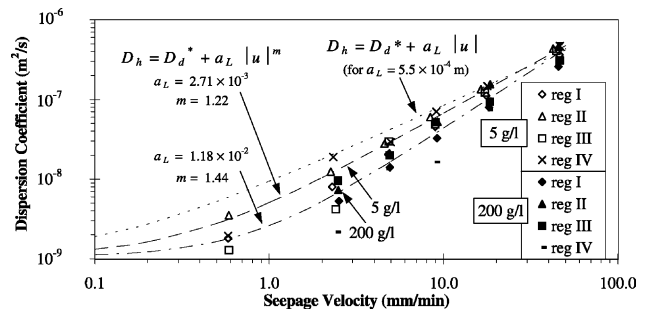


Fig. 21. Fitted hydrodynamic dispersion coefficients for the CS5–CS10 displacements.

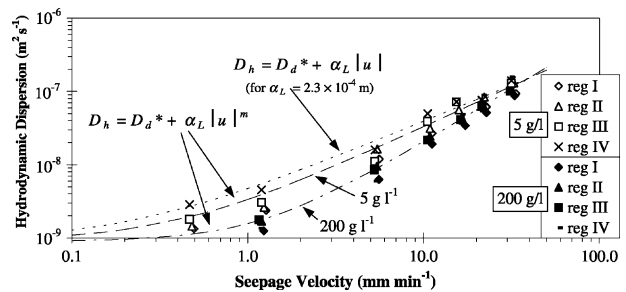


Fig. 22. Fitted hydrodynamic dispersion coefficients for the MS1–MS7 displacements.

the range given, i.e. $\alpha_L = 1.18 \times 10^{-2} m$, $m = 1.44$. This indicated that the disparity in the fitted dispersion coefficients was not solely due to apparatus-induced dispersion in the low concentration displacements, but rather that the classical formulation of Fick’s law did not adequately describe the dispersion in the 200 g l⁻¹ displacements.

The nonlinear hydrodynamic dispersion equation for low concentration solute dispersion—i.e., taking $D_d^* = 1.08 \times 10^{-9}$, m² s⁻¹, $a_L = 2.71 \times 10^{-3} m$ and $m = 1.22$ in (14)—determined for coarse sand was used for further analyses in Section 6.3.

The hydrodynamic dispersion results obtained from the constant flow rate displacements in medium sand were similar to those obtained from the coarse sand tests. See Fig. 22 for details.

The fitted longitudinal dispersivity value obtained for the 5 g l⁻¹ displacements was 0.54 mm which is the same order of magnitude as the average grain size (0.27 mm) for the medium sand. However, the longitudinal dispersivity fitted to the 200 g l⁻¹ results was 7.1 mm which is much larger. The exponent value for the 5 g l⁻¹ displacement was 1.17 which was in the range indicated by previous experimental results, however the exponent for the 200 g l⁻¹ displacements (1.47) was significantly higher than 1.2, the maximum in the range obtained previously. The large dispersivity and exponent values obtained for the 200 g l⁻¹ displacements indicate that

apparatus-induced dispersion in the low concentration displacements was not the sole cause of the disparity between the low and high concentration dispersion results.

6.3. Applicability of Fick’s law

The effect of concentration on solute dispersion is not included in the classical formulation of Fick’s law or the classical theory for density-dependent solute transport. However, the hydrodynamic dispersion results show that the influent solution concentration does affect solute dispersion. In particular, dispersion is suppressed as the influent solution concentration increases.

6.3.1. Nonlinear dispersion theory

The nonlinear dispersion Eq. (1) was incorporated into the density-dependent solute transport model presented in Section 2 to form a β -modified numerical model. A number of numerical simulations were then run for a range of β values for both low and high influent solution concentrations. The parameters and boundary conditions used in the simulations were based upon the experimental conditions for the coarse sand displacements conducted at a constant influent flow rate (CS5–CS10).

Numerical experiments showed that, over a range of β values, the high concentration breakthrough curves were less dispersed than the corresponding low concentration breakthrough curves. That is, the effect of the nonlinear dispersion Eq. (1) is to reduce the dispersion of the solute front in the high concentration displacements whilst not affecting dispersion in the lower concentration displacements. This trend corresponded to that observed in the experimental results.

The β -modified numerical model was incorporated into the least-squares optimisation program [27]. As mentioned already, the fitted hydrodynamic dispersion expression for the coarse sand experiments was used throughout.

Numerical solute breakthrough curves using the modified numerical model were then fitted to the level L5 experimental solute breakthrough curves from the 200 g l⁻¹ constant flow rate displacement experiments in coarse and medium sand to obtain a fitted β value for each experiment. Fig. 23 shows the fitted numerical and experimental solute breakthrough curves for three different 200 g l⁻¹ displacements in coarse sand. The breakthrough curves in Fig. 23 show that the shape of the numerical solute breakthrough curves agreed well with the experimental breakthrough curves. This indicated that the nonlinear dispersion theory adequately predicted the shape of the solute breakthrough curves.

The variation of the fitted β values with flow rate was then examined. The fitted β values from the 200 g l⁻¹ displacements in coarse and medium sand are plotted

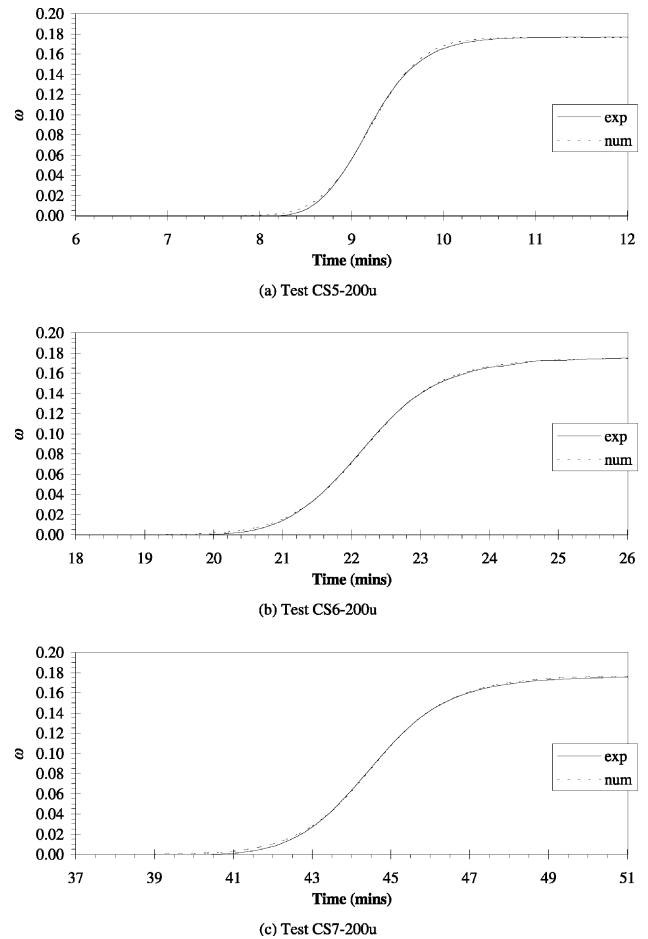


Fig. 23. Level L5 experimental and fitted, β -modified, numerical solute breakthrough curves. Test (a) CS5-200u, (b) CS6-200u, (c) CS7-200u.

against seepage velocity in Fig. 24. The results presented in Fig. 24, particularly for the coarse sand displacements, show that β varies almost linearly, and inversely with the seepage velocity in log–log space. The following

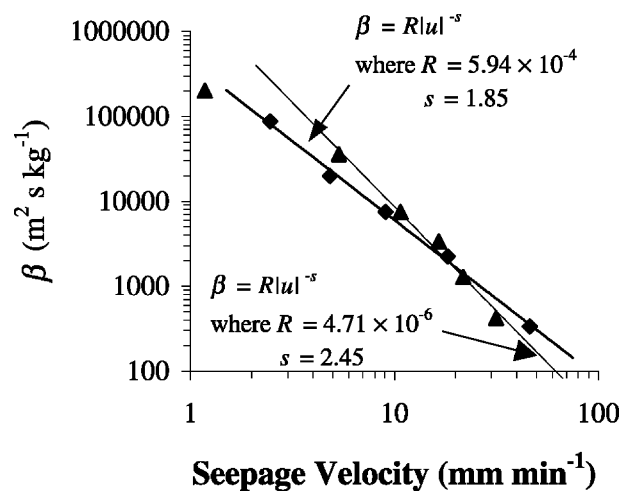


Fig. 24. Fitted β values for the 200 g l⁻¹ coarse (♦) and medium (□) sand displacements.

equation was used to fit a curve to the results and is shown by the curves in Fig. 24:

$$\beta = R|u|^{-s}. \quad (15)$$

The β values determined for the medium sand tests did not show the same linearity with seepage velocity in log–log space as those obtained from the coarse sand results. At the low seepage velocity of 1.2 mm min^{-1} the β value was significantly lower than expected if the results were to form a straight line in log–log space. The grain Péclet number for this test was 2.4, indicating that the spreading caused by molecular diffusion and mechanical dispersion was of a similar order of magnitude. It is possible that β , like the hydrodynamic dispersion coefficient, becomes a constant at the lower seepage velocities when molecular diffusion is the dominant spreading mechanism. The grain Péclet number corresponding to the slowest coarse sand result in Fig. 24 was 14.7. Mechanical dispersion was therefore the dominant spreading mechanism in all of the coarse sand tests, so a diffusion effect was not apparent in the results.

Although the β curve for medium sand did not show the same linearity as apparent for the coarse sand, the results presented in Fig. 24 indicate that the values determined for β were similar for the two soils, with only a minor dependence on soil type. The β values were lower at higher seepage velocities and increased in value with decreasing seepage velocity. These results indicated that, at higher seepage velocities, dispersion of a high concentration solute front was only slightly less than the dispersion of a low concentration solute front. However, as the seepage velocity reduced, the difference in dispersion of a high and low concentration solute front became more significant.

For a possible physical explanation for the reduction of dispersion for high concentration displacements we refer to [23]. The hypothesis presented in [23] assumes that the reduction of hydrodynamic dispersion under high-concentration-gradient conditions is the result of the interplay between gravity and local horizontal density gradients. These horizontal gradients are due to local inhomogeneities of porous medium properties like intrinsic permeability and porosity. At low average flow rates, the stabilizing effect of gravity is expected to be more pronounced than under high average flow rate conditions. The results shown in Fig. 24 confirms this behaviour. The nonlinear dispersion parameter β decreases linearly with the average seepage velocity on a log–log scale. This is consistent with the results presented in [23].

This aforementioned explanation is also consistent with previous experimental results (e.g., [14]) obtained using miscible fluids of differing density and viscosity ratios which found that dispersion was reduced if the density and viscosity ratios of the displacing and produced fluid were such that the displacement was

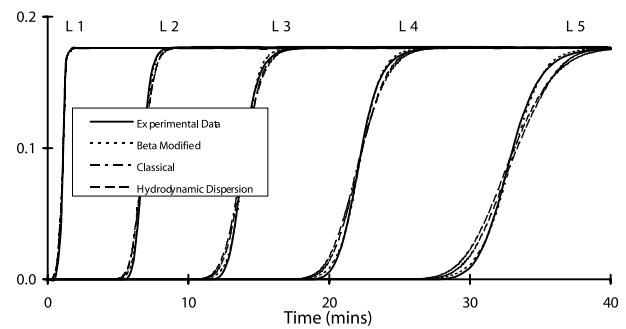


Fig. 25. Comparison of the 200 g l^{-1} CS4 experimental breakthrough curves with numerical breakthrough curves from the nonlinear analysis and classical analysis.

stable. Furthermore, the greater the contrast in the stable configuration the less the dispersion of the solute front.

6.3.2. Testing the nonlinear dispersion theory

A final investigation was conducted to assess the applicability of the nonlinear dispersion theory to high concentration (gradient) displacements. The results of this extensive analysis confirmed the validity of the nonlinear extension of Fick's law contained in (1). It gives rise to a model that accurately describes the fluid flow and solute transport processes involved in low and high concentration contaminant transport through saturated, coarse- and medium-grained sands. Moreover, the results are consistent with the results obtained by [23]. They found an expression for the variation of β with the seepage velocity, similar to (15), under the assumption of the validity of classical (nonextended) Darcy law.

The present study confirms the correctness of this assumption. Both the results of constant flow rate and constant head tests were used to assess the applicability of the nonlinear dispersion theory. In particular, the constant head tests provided useful data for validation purposes, because the flow rate varied significantly for the tests conducted with higher influent solution concentrations. The breakthrough curves for the 5, 50 and 200 g l^{-1} displacements from the CS1 and CS4 tests were selected for comparison with the modified theory, to cover the range of influent solution concentrations tested and a range of seepage velocities. Computed and measured breakthrough curves for the 200 g l^{-1} CS4 test are given in Fig. 25.

7. Conclusions

The major conclusions arising from this analysis of stable, brine displacements are summarised below:

1. Darcy's law was found to be applicable to high concentration solute transport through saturated coarse-grained soils.

2. The hydrodynamic dispersion coefficient was found to be a nonlinear function of the seepage velocity.
3. The modification to Fick's law proposed by [11] was found to accurately predict both low and high concentration solute transport through saturated coarse grained soils. Fick's law without the modification gave less accurate and inconsistent predictions of the experimental data.
4. The additional dispersion parameter, β , contained in the modified Fick's law was found to vary linearly with the seepage velocity in log–log space when mechanical dispersion was the dominant spreading mechanism.
5. β varied only a small amount between coarse and medium sands, suggesting that, at least for unconsolidated, granular media, it is only slightly dependent on medium properties.
6. β decreases with increasing flow rate, density and viscosity contrasts, consistently with the notion that these factors act to stabilise perturbations at the interface of the displacing and displaced solutions.

References

- [1] Anderson SJ. An experimental investigation of high concentration displacements in saturated porous media. Ph.D. thesis, Department of Civil Engineering, The University of Western Australia, Nedlands, Western Australia, Australia, 1997.
- [2] Anderson SJ, Barry DA. Experimental investigation of brine transport through sand. In: Bouazza A, Kodikara J, Parker R, editors. *Environmental Geotechnics: Proceedings of the 1st Australia–New Zealand Conference on Environmental Geotechnics–Geoenvironment 97*, Melbourne, Victoria, Australia, 26–28 November. Rotterdam, Brookfield: A.A. Balkema; 1997. p. 353–8.
- [3] Anderson SJ, Barry DA, Culligan-Hensley PJ. Experimental evaluation of a brine transport model. In: Kamon M, editor. *Environmental Geotechnics: Proceedings of the Second International Congress on Environmental Geotechnics Osaka, Japan*, 5–8 November. Rotterdam: A.A. Balkema; 1996. p. 193–8.
- [4] Barry DA, Parlange J-Y, Starr JL. Numerical analysis of the precursor effect. *Soil Sci* 1987;143:309–17.
- [5] Barry DA, Starr JL, Parlange J-Y, Braddock RD. Numerical analysis of the snow-plow effect. *Soil Sci Soc Am J* 1983;47: 862–8.
- [6] Brigham WE, Reed PW, Dew JN. Experiments on mixing during miscible displacements in porous media. *Soc Petrol Eng J* 1961;1:1–8.
- [7] Harleman DRF, Melhorn PF, Rumer RR. Dispersion-permeability correlation in porous media. *J Hydraul Div, ASCE* 1963;89:67–85.
- [8] Hassanizadeh SM. Experimental study of coupled flow and mass transport: a model validation exercise. In: Kovar K, editor. *ModelCARE 90: Calibration and Reliability in Groundwater Modelling*. Washington DC and Paris: IAHS Publ. No. 195; 1990. p. 241–50.
- [9] Hassanizadeh SM, Leijnse A, DeVries WJ, Stapper RAM. Intraval, test case 13: Experimental study of brine transport in porous media. Technical Report 725206003. RIVM, Bilthoven, The Netherlands, 1990.
- [10] Hassanizadeh SM, Leijnse T. On the modelling of brine transport in porous media. *Water Resour Res* 1988;24:321–30.
- [11] Hassanizadeh SM, Leijnse T. A non-linear theory of high-concentration gradient dispersion in porous media. *Adv Water Resour* 1995;18:203–15.
- [12] Head MJ. The use of miniature four-electrode conductivity probes for high resolution measurement of turbulent density or temperature variations in salt-stratified water flows. Unpublished Ph.D. thesis, University of California, San Diego, 1983.
- [13] Hill S. Channelling in packed columns. *Chem Eng Sci* 1952;1:247–53.
- [14] Kempers LJTM. Dispersive mixing in stable and unstable miscible displacements. Unpublished Ph.D. thesis, Delft University of Technology, Delft, The Netherlands, 1991.
- [16] Marquardt DW. An algorithm for least-squares estimation of nonlinear parameters. *J Soc Ind Appl Math* 1963;11:431–41.
- [17] Mitchell JK. Conduction phenomena: from theory to geotechnical practice. *Géotechnique* 1991;41:299–340.
- [18] Mohanty KK, Ottino JM, Davis HT. Reaction and transport in disordered composite media: introduction of percolation concepts. *Chem Eng Sci* 1982;37:905–24.
- [19] Moser H. Einfluß der Salzkonzentration auf die Hydrodynamische Dispersion im Porösen Medium. Ph.D. thesis, Technische Universität Berlin Report No. 128.
- [20] Noye J. Finite difference methods for partial differential equations. In: Noye J, editor. *Numerical Solutions of Partial Differential Equations*. New York: North-Holland; 1982.
- [21] Parker JC, van Genuchten MTh. Determining transport parameters from laboratory and field tracer experiments. *Bulletin* 84-3, Virginia Agricultural Experiment Station, Blacksburg, Virginia, 1984.
- [22] Rumer RR. Longitudinal dispersion in steady and unsteady flow. *J Hydraul Div, ASCE* 1962;88:147–72.
- [23] Schotting RJ, Moser H, Hassanizadeh SM. High-concentration-gradient dispersion in porous media: experiments, analysis and approximations. *Adv Water Resour* 1999;22:655–80.
- [24] Slobod RL, Howlett WE. The effects of gravity segregation in laboratory studies of miscible displacement in vertical unconsolidated porous media. *Soc Petrol Eng J* 1964;4:1–8.
- [25] Standards Australia. Methods of testing soils for engineering purposes—Soil classification tests—Determination of the particle size distribution of a soil—Standard method of analysis by sieving. AS1289.3.6.1, 1995.
- [26] Voss CI. SUTRA, Saturated–unsaturated TRANsport. A finite-element simulation model for saturated–unsaturated, fluid-density-dependent ground-water flow with energy transport or chemically-reactive single-species solute transport. Technical report, Water-Resources Investigations Report 84-4369, Reston, Virginia, 1984.
- [27] Watson SJ, Barry DA. Numerical analysis of stable brine displacements for evaluation of density-dependent flow theory. *Phys Chem Earth Part B* 2001;26:433–40.
- [28] Watson SJ, Barry DA, Schotting RJ, Hassanizadeh SM. On the validity of the Darcy's Law for stable high-concentration displacements in granular porous media. *Trans. Porous Media*, in press.
- [29] Watson SJ, Culligan PJ. The development of small-scale conductivity probes for solute transport experiments. Technical Report G1455, Geoemchanics Group, Department of Civil Engineering, The University of Western Australia, Nedlands, Western Australia, 1999.

- [30] Weast RC. CRC Handbook of chemistry and physics. Cleveland, Ohio, USA: CRC Press Inc; 1977.
- [31] Yeung AT, Mitchell JK. Coupled fluid, electrical and chemical flows in soil. *Géotechnique* 1993;43:121–34.
- [32] Yong RN, Warkentin. Developments in geotechnical engineering. In: Aravind B, editor. *Principles of Contaminant Transport in Soils*, vol. 73. Amsterdam, The Netherlands: Elsevier Science Publishers; 1992.